Nanoscale

ROYAL SOCIETY OF CHEMISTRY

REVIEW

View Article Online
View Journal | View Issue

Cite this: *Nanoscale*, 2022, **14**, 3306

Recent development of a magneto-optical nanoplatform for multimodality imaging of pancreatic ductal adenocarcinoma

Xuan Zhang,[a,b] Zhiming Zeng,[a,b] Huiyi Liu,[a] Li Xu,[a] Xin Sun,[c] Jing Xu*[b] and Guosheng Song *[a]

Pancreatic ductal adenocarcinoma (PDAC) is the most common type of pancreatic cancer. Given its inconspicuous and atypical early symptoms and hidden location, most patients have already reached the terminal stage before diagnosis. At present, the diagnosis of PDAC mainly depends on serological and imaging examinations. However, serum tests cannot identify specific tumor locations and each imaging technology has its own defects, bringing great challenges to the early diagnosis of PDAC. Therefore, it is of great significance to find new strategies for the early and accurate diagnosis of PDAC. In recent years, a magneto-optical nanoplatform integrating near infrared fluorescence, photoacoustic, magnetic resonance imaging, *etc.* has attracted widespread attention, giving full play to the complementary advantages of each imaging modality. Herein, we summarize the recent advances of imaging modalities in the diagnosis of pancreatic cancer, and then discuss in detail the construction and modification of magneto or/and optical probes for multimodal imaging, and advances in early diagnosis using the combination of various imaging modalities, which can provide potential tools for the early diagnosis or even intraoperative navigation and post-treatment follow-up of PDAC patients.

Received 22nd December 2021,
Accepted 24th January 2022

DOI: 10.1039/d1nr08394e

rsc.li/nanoscale

[a]*State Key Laboratory of Chemo/Biosensing and Chemometrics, College of Chemistry and Chemical Engineering, Hunan University, Changsha 410082, P. R. China. E-mail: songgs@hnu.edu.cn*
[b]*Department of Ophthalmology and Otolaryngology, National Clinical Research Center for Geriatric Disorders, Xiangya Hospital, Central South University, Changsha 410008, P. R. China. E-mail: xujing1981@csu.edu.cn*
[c]*College of Mechanical and Electrical Engineering, Central South University, Changsha 410083, P. R. China*

Guosheng Song

Guosheng Song is a professor at Hunan University in China. He received his PhD degree from Donghua University in 2014. He did his postdoctoral research at Soochow University and then at Stanford University from 2014 to 2018. In 2018, he joined the College of Chemistry and Chemical Engineering, Hunan University. His research mainly focuses on the design of activatable nanoplatforms for multimodal imaging and cancer specific therapy.

1. Introduction

Pancreatic ductal adenocarcinoma (PDAC) is the most prevalent and aggressive primary malignancy of the pancreas, with an overall 5-year survival rate of less than 10%, making it one of the deadliest types of cancers in the world.[1,2] In the United States, pancreatic carcinoma is estimated to cause over 20 000 deaths in both genders in 2021, ranked third after pulmonary cancer, breast or prostate cancer and colorectal cancer.[3] The most important factor determining the prognosis of tumor patients is their clinical stage.[1] Unfortunately, the majority of PDAC patients have already reached the terminal-stage before diagnosis, as a result of the inconspicuous and atypical early symptoms and hidden location of this type of malignant tumor.[4,5] The 5-year survival rate of early-stage patients is approximately 60 times higher than that of terminal-stage patients.[6] Therefore, improving the early diagnosis rate of PDAC patients is the key to increasing their five-year survival rate.[7,8]

At present, PDAC continues to exhibit a poor prognosis due to the difficulty in early diagnosis.[9,10] The pancreas is a retroperitoneal organ located posterior to the stomach, between the spleen and the duodenum. Due to the interference of gases in the gastrointestinal tract, it is difficult to obtain clear and high-quality images of the early primary

tumor and its distant metastasis accurately using the current clinical examination methods.[11] Moreover, the present commonly used clinical diagnostic methods (serological and imaging examinations) have their own limitations. Specifically, CEA and CA19-9 are unable to determine the tumor location; in addition, the sensitivity and speciality of these two cancer antigens are not ideal.[8,12,13] Computed tomography (CT) imaging has difficulties in detecting microtumors less than 1 cm in diameter, differentiating benign and malignant lesions, and displays the disadvantage of ionizing radiation.[14,15] Magnetic resonance imaging (MRI) has the shortcomings of long scanning time, high cost and low sensitivity in the detection of PDAC.[16] Endoscopic ultrasound imaging (EUS) has successfully detected PDAC microtumors in some areas, but is heavily dependent on the dexterity of the operator and the condition and cooperation of the patient, and has an average detection rate lower than 50% when microtumors are smaller than 1 cm in diameter.[17,18] Moreover, contrast media used in CT and MRI scanning are nephrotoxic and can hardly enter PDAC tissue due to the high interstitial fluid pressure and low microvessel density.[19–21] Therefore, it is of great significance to develop new strategies for the early and accurate diagnosis of PDAC.[22,23]

In order to overcome the above difficulties, various magneto-optical nanoplatforms integrating fluorescence imaging, photoacoustic imaging, magnetic resonance imaging, *etc*. have been designed.[24] These magneto-optical nanoplatforms can specifically target PDAC cells *via* recognition of specific molecular receptors or the urokinase-type plasminogen activator receptor (uPAR) and cell-surface associated mucin 1 (MUC1), which are highly expressed specifically in PDAC cells.[25] A magneto-optical nanoplatform can also be designed to respond to specific biomarkers, including pH, oxidative stress, metal ions, anoxia and specific enzymes such as matrix metalloproteinases (MMPs).[19,26] Furthermore, the magneto-optical nanoplatform have a longer circulation time in blood compared to conventional contrast medium, along with the advantage of strong signal expression in lesions in multi-imaging modalities such as MRI, fluorescence imaging (FI) and photoacoustic imaging (PAI), thus achieving long term and high contrast multimodality imaging of PDAC. This technology overcomes the limitations of traditional imaging examinations, showing higher sensitivity and specificity, therefore bringing hope to achieve a higher early and accurate diagnosis rate of PDAC, and offers a great value in intraoperative navigation and post-treatment follow-up of PDAC patients.

In this review, we summarized the advances in recent years regarding imaging modalities in the diagnosis of pancreatic cancer, and discussed in detail the construction and modification of probes for the magneto-optical nanoplatform, the advances and potential application of the magneto-optical nanoplatform in the early diagnosis of PDAC, as well as the future development and challenges of this novel imaging method (Fig. 1).

2. Imaging modalities in the diagnosis of PDAC

Currently, there are no reliable blood markers that can diagnose early-stage PDAC, which is also often asymptomatic. Therefore, medical imaging plays an important role in the early diagnosis of PDAC. Common clinical imaging methods for the diagnosis of PDAC include ultrasound (US), CT, MRI, and EUS. In this part, we summarize the characteristics and limitations of the current imaging methods applied in the diagnosis of PDAC, and potential imaging modalities for the early diagnosis of PDAC, along with recent advances in nanomaterials modified for the single-modality imaging of PDAC (Fig. 2).

2.1. Overview of imaging modalities in PDAC diagnosis

2.1.1. Current imaging modalities applied in PDAC diagnosis. Transabdominal US is commonly used in the diagnosis of PDAC, using the principle of the "Doppler effect" or echoes to convert reflected sound energy into images, with a sensitivity of 75 to 89% and specificity of 90–99% in the detection of PDAC masses.[1] Moreover, US shows great sensitivity in distinguishing non-obstructive jaundice and obstructive jaundice, which is a common feature in patients with PDAC, and therefore is often initially performed in patients with symptoms of jaundice or upper abdominal pain. However, due to the anatomical location of the pancreas, imaging quality is affected by bowel gas. EUS is not subjected to this limitation, and has the advantage of being able to obtain a tissue biopsy during an examination. EUS is also of particular importance in the detection of small masses less than 2 cm in diameter, often seen in patients of high clinical suspicion but lacks a detectable mass on other imaging modalities.[27] EUS has a sensitivity of about 87% and specificity of around 98% in detecting PDAC, and has successfully detected PDAC microtumors in some areas, but the detection rate of microtumors which are less than 1 cm in diameter is still lower than 50%.[28,29] Furthermore, EUS is an invasive imaging method, making patients nervous or antipathetic towards the examination, and both US and EUS depend greatly on the operator experience and patient cooperation.

CT is often seen as the initial imaging method for evaluating patients suspected with PDAC, with an overall sensitivity of about 89% and specificity of around 90%.[30] CT uses ionizing radiation or X-ray beams that rotate around and pass through the patient, in combination with an electronic detector array that records the detected density patterns and generates images of a "slice" or "cut" of tissues through complex reconstruction methods.[31] CT is the best modality for the assessment of locoregional and nodal pancreatic tumors and has been validated as the reference standard. Moreover, triphasic cross-sectional imaging and the use of thin slices can be used to assess respectability and visualize important vessels and anatomic relationships. However, CT has the disadvantage of ionizing radiation, and PDAC microtumors are often over-

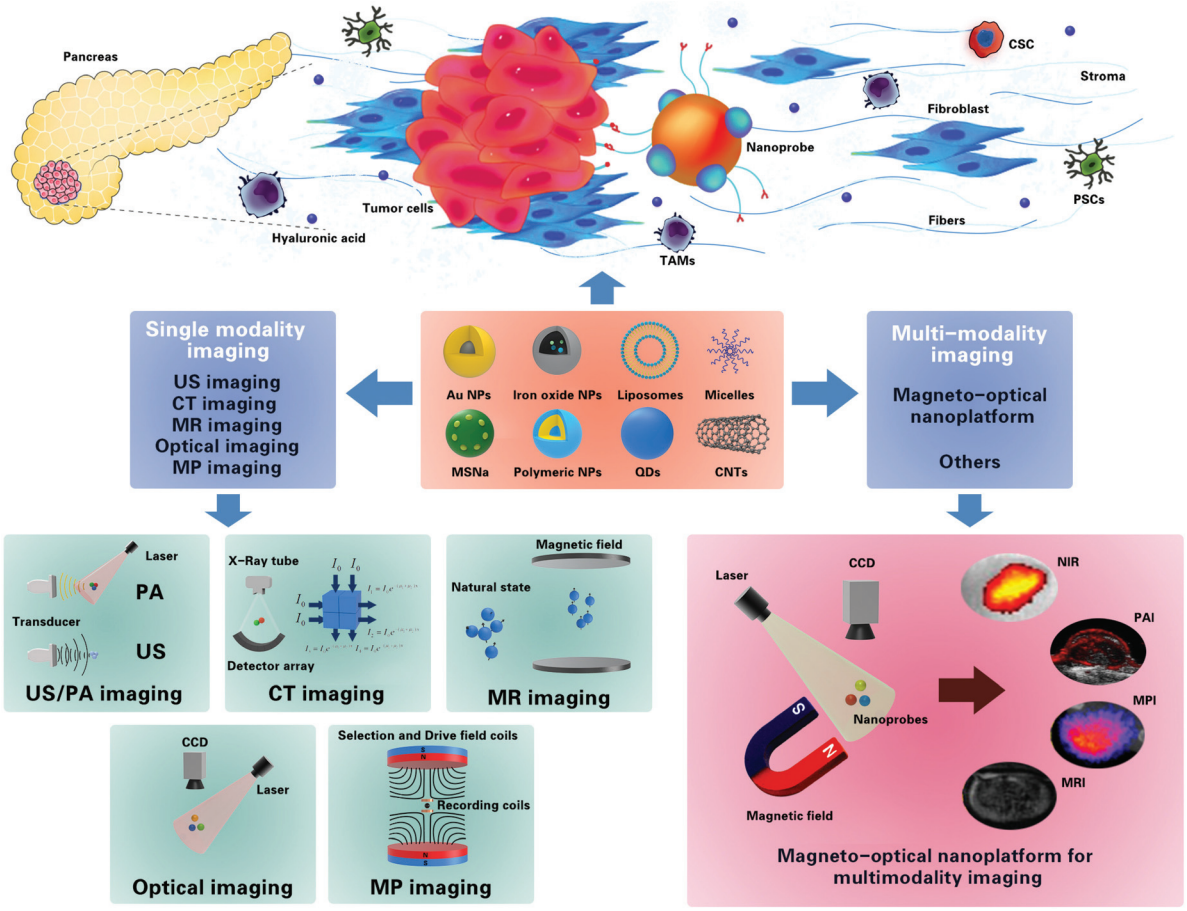

Fig. 1 Illustration of various nanoparticles that can be easily modified or loaded with imaging agents for imaging of PDAC, and their use in various imaging modalities for the diagnosis of DPAC.

looked on CT, with a reported sensitivity of only 58%–77% when masses are less than 2 cm in diameter.[27,32] Positron-emission tomography (PET)/CT has been gradually applied to early diagnosis of PDAC, but remains a controversial modality, with the reported high detection rates of PDAC tumors being smaller than 2 cm diameter of 81–100%, yet also low sensitivity to 50% in other reported studies.[33,34]

Magnetic resonance imaging (MRI) is one of the most widely used imaging methods in hospitals and clinics for medical diagnosis, staging and follow-up of disease, with a reported PDAC diagnosis specificity equivalent to CT of about 89%.[35] MRI is based on the excitement and detection of the change in the direction of the rotational axis of protons found in the water forming living tissues, with the advantages of high spatial resolution, unlimited tissue penetration and no involvement of X-rays or use of ionizing radiation, and therefore serves as a great alternative when imaging methods such as US, X-ray and CT cannot accurately detect lesions and assess disease progression, especially of soft tissues of the brain or abdomen.[36] MRI can comprehensively obtain sectional images in any direction, three-dimensional volume images, and even four-dimensional images of spatial spectral distribution, including qualitative information such as the characteristics of anatomical structures of tissues and organs, tumor blood supply and tumor vascular distribution, and therefore can be used to accurately detect and locate tumors as well as monitor tumor growth. However, MRI has a limited value in distinguishing PDAC from mass-forming chronic pancreatitis, and as with CT imaging, MRI is weak in detecting microtumors.[16]

2.1.2. Potential imaging modalities for PDAC diagnosis. Optical imaging, an emerging molecular imaging method, has received extensive attention from researchers and has increasingly shown great potential in the early diagnosis of PDAC as an alternative method.[37] Compared with traditional imaging methods, optical imaging displays the advantages of high sensitivity, simple operation and no radioactivity. In addition, optical imaging can detect abnormalities at the cellular or molecular level before tumor cells develop and progress into solid tumors that invade and damage surrounding tissues.[38] Optical imaging can also inspect single tumor cells in real-time, and provide real-time visualization of primary tumor lesions, sentinel lymph node lesions and lesions in surrounding tissues, and therefore can successfully detect microtumors that are less than 1 cm in diameter so as to achieve an early diagnosis of PDAC.[39] Optical imaging can not only be applied

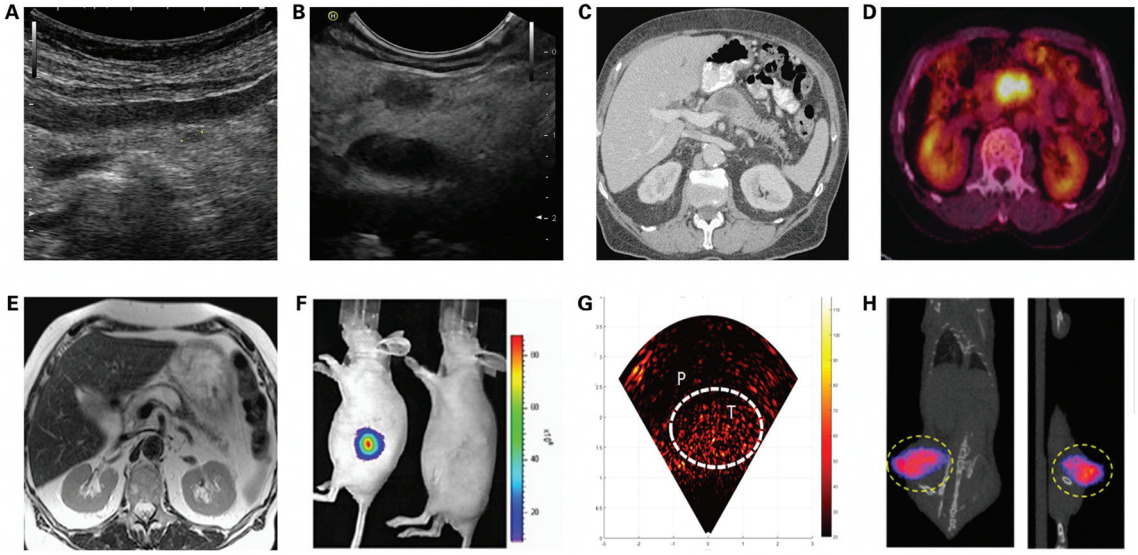

Fig. 2 Single imaging modalities for the diagnosis of PDAC, including (A) transabdominal ultrasound imaging; (B) endoscopic ultrasound imaging. Reproduced with permission from ref. 120. Copyright 2020. KSUM; (C) computed tomography. Reproduced with permission from ref. 141. Copyright 2008. Elsevier; (D) positron-emission tomography/CT. Reproduced with permission from ref. 142. Copyright 2018. The Authors. Licensee IntechOpen; (E) magnetic resonance imaging. Reproduced with permission from ref. 141. Copyright 2008. Elsevier; (F) optical imaging-NIR. Reproduced with permission from ref. 143. Copyright 2015. Elsevier; (G) optical imaging-PAI. Reproduced with permission from ref. 144. Copyright 2019. Elsevier; (H) magnetic particle imaging. Reproduced with permission. Copyright 2019. ACS.

to the early diagnosis of PDAC, but also shows great value and accuracy in the application of tumor classification and staging; preoperative determination of the resection extent, intraoperative guidance of precise tumor resection, so as to reduce the surgical margin range, operation duration and surgical trauma; postoperative monitoring of tumor recurrence and postoperative evaluation of the treatment effect through imaging-guidance.[40,41] Optical imaging for preclinical or clinical diagnosis is mainly composed of photoluminescence (PL), chemiluminescence (CL), surface-enhanced Raman spectroscopy (SERS), and photoacoustic imaging (PAI), which will be elaborated respectively in the following contents.[42]

At present, PL is the most commonly used method in optical imaging. PL probes include quantum dots, lanthanide NPs, fluorescence dye, *etc*., amongst which fluorescence imaging is the most widely used in the clinic.[42] The basic principle of fluorescence imaging is to inject a combination of optical nanoparticles and fluorescent dyes into cells or animals; the combination absorbs light at a certain wavelength range, and the electrons in optical nanoparticles are then excited to a higher and more unstable energy state, relaxes to their ground state and emits a photon of light of a specific wavelength range which can be detected using a fluorescence imaging system, so as to achieve tracking, and qualitative and quantitative analysis of optical nanoparticles.[43]

Chemiluminescence is a kind of optical radiation phenomenon where light is generated through chemiexcitation during the process of the chemical reaction, in which substances are activated by oxidation and form an unstable oxidized highly energetic intermediate, which decomposes or transfers energy to the neighboring fluorophores, and relaxes to its ground state, during which it emits luminescence.[44,45] Unlike traditional fluorescence imaging methods, which suffer from photobleaching and autofluorescence, CL eliminates excitation light, thereby permitting deep-tissue imaging with ultrahigh sensitivity and no background noise from biological tissues.[46–49]

Raman spectroscopy (RS) has gained enormous interest as a physicochemical technique, due to its outstanding chemical specificity during identification and quantification of specific substances, providing vibration fingerprint-like spectra of chemical and biological materials without interference from water.[50] However, non-resonant RS is a weak scattering technique, limiting its development in clinical imaging. Surface-enhanced Raman spectroscopy (SERS) can provide up to 108 enhancement of the Raman signal, allowing the detection of low concentration analytes, showing great potential as an excellent tool for clinical diagnosis.[51]

Photoacoustic imaging (PAI), also called optoacoustic imaging, is a novel biomedical imaging method based on the use of laser-generated ultrasound that has emerged over the last decade, which combines the advantages of optical imaging and ultrasound imaging, showing both high contrast and high spatial resolution in imaging, bringing great potential and expectation for the early diagnosis of PDAC.[52–54] In PAI, based on the photoacoustic effect, modulated electromagnetic radiation is pulsed to biological tissue. The irradiated tissue then expands rapidly after absorption of laser energy

due to thermoelasticity and excites broadband ultrasound waves, which provide high contrast, high temporal and spatial resolution, and non-invasive images.[55–57] In contrast to fluorescence imaging, the acoustic signal of PAI is positively correlated with the optical absorption intensity of imaging tissues, instead of relying on the detection of emitted light from imaging tissues, providing PAI with a greater penetration depth than pure optical imaging modalities like FI.[58–60]

As a magnetic imaging modality, unlike MRI, magnetic particle imaging (MPI) directly maps the spatial distribution of magnetic nanoparticle contrast agents *in vivo* using a time-varying magnetic field, instead of indirectly mapping through the MRI signal.[61] MPI exploits the magnetization characteristic of nanoparticle contrast agents to localize the spatial distribution of the nanoparticles, and therefore the sensitivity and resolution of MPI are determined by nanoparticle contrast agent characteristics, showing great potential of development with the advances of materials science. MPI also shows great potential in clinical imaging with a near-perfect contrast, and no obscuring background tissue, due to zero manifesting of the MPI signal from human tissue which is diamagnetic. Moreover, MPI is quantitative at any depth with low-frequency magnetic fields where there is zero depth attenuation.[62–64] The above advantages make MPI an excellent alternative in PDAC diagnosis over standard imaging techniques CT and MRI.

2.2. Advances in nanomaterials for single-modality imaging of PDAC

Imaging examination plays an important role in the clinical diagnosis of PDAC, popular imaging techniques include CT, MRI, US and EUS. However, each imaging technology has its own defects, particularly in the detection of microtumors less than 1 cm in diameter or depending too much on the operator experience and patient condition, bringing great challenges to the early diagnosis of PDAC. With the use of contrast agents, healthy tissue and lesions can be better distinguished. However, traditional contrast agents suffer from several drawbacks and limitations, such as lack of specificity and organ toxicity, leading to a focus of attention from researchers on novel nanomaterials.[65] Nanoprobes have the advantages of small size, strong targeting ability, great degradability, and little stimulation to biological tissues. They can also be synthesized with different coatings that can be modified to include various desirable functionalities, showing great potential as an auxiliary means for the early diagnosis of PDAC.[66,67] Recent advances in nanoprobes for single-modality imaging of PDAC will be introduced in the following contents.

2.2.1. Optical imaging. Optical imaging has attracted much attention from materials science researchers as an emerging molecular imaging method, showing great potential in the early diagnosis of PDAC. At present, fluorescence imaging (FI) is one of the most commonly used methods in optical imaging for the early diagnosis of PDAC.[43] In recent years, a large number of studies have been carried out regarding the optical imaging of PDAC using near-infrared (NIR) fluorescent dyes, peptide NP, Au NPs and Cu NPs. Amongst them, near-infrared fluorescence imaging is the most frequently used fluorescence imaging method in optical imaging.[68,69] Whereas the visible spectrum (VIS), which ranges from 400 nm to 650 nm, penetrates through tissue on a micron scale, NIR fluorescent light ranging from 650 to 2000 nm can travel up to 2–4 cm deep, due to the low absorption and scattering of light as well as the very little exhibition of autofluorescence in the NIR spectrum in tissue. In recent years, advances in biomedical FI in the NIR region mainly focused on the traditional NIR window (NIR-I; λ = 700–900 nm), which hindered the further application of FI in deep tumors, and therefore the NIR region has recently been extended to the second NIR window (NIR-II; λ = 1000–1700 nm).[70–73] Commonly used near infrared dyes include indocyanine Green (ICG), IR780, IR820 and cyanide dyes (cy5.5, cy7, cy7.5, *etc.*).[74–76] However, current fluorophores lack high quantum efficiency and tumor targeting ability, causing a dominant barrier to the extensive approvement of NIR dyes in clinical application.[77] In order to promote clinical translation of NIR bioimaging, small molecule-derived nanoprobes have attracted extensive attention. These novel nanoprobes can also be synthesized with different coatings that can be modified to include various desirable characteristics and functionalities, such as higher biocompatibility, cancer targeting, or even cancer treatment.[78] Recent advances of NIR dye synthesized nanoprobes will be discussed in detail respectively in the following contents.

Hyaluronic acid (HA) is a substance naturally produced by the human body, serves as a component of the extracellular matrix, is mainly produced to retain water and lubricate tissues, and participates in cell proliferation, healing of wounds, and cancer metastasis.[78–80] Self-assembled HA nanoparticles have been extensively investigated by researchers as cancer diagnosis and treatment agents due to their biocompatibility, biodegradability and targeting characteristics.[81,82] Qi *et al.* designed a PDAC targeted ICG nanoprobe termed NanoICG, by physiochemically entrapping indocyanine Green into hyaluronic acid derived nanoparticles, intended for the detection of pancreatic cancer[83] (Fig. 3A–C). Contrast-enhancement of pancreatic cancer by NanoICG was verified *in vivo*, and unlike traditional contrast agents that can hardly enter the PDAC tissue, NanoICG can accumulate significantly in PDAC tissue through the EPR effect and demonstrate contrast-enhancement for pancreatic lesions relative to disease-free portions of the pancreas, with negligible cytotoxicity to healthy pancreatic epithelial cells and nearly no signs of chemotaxis or phagocytosis, suggesting that NanoICG is a promising potential contrast agent for the early detection of PDAC and intraoperative guidance of tumor removal.

Calcium phosphosilicate nanoparticles (CPSNPs) were developed to deliver imaging agents and drugs for the diagnosis and treatment of human cancer.[84,85] This material is an amorphous calcium phosphate, designed to encapsulate particles of various shapes and sizes, including chemotherapeutics and imaging agents such as indocyanine Green. This particle has the advantages of small size, being biocompatible and biodegradable, are able to remain intact in blood but dis-

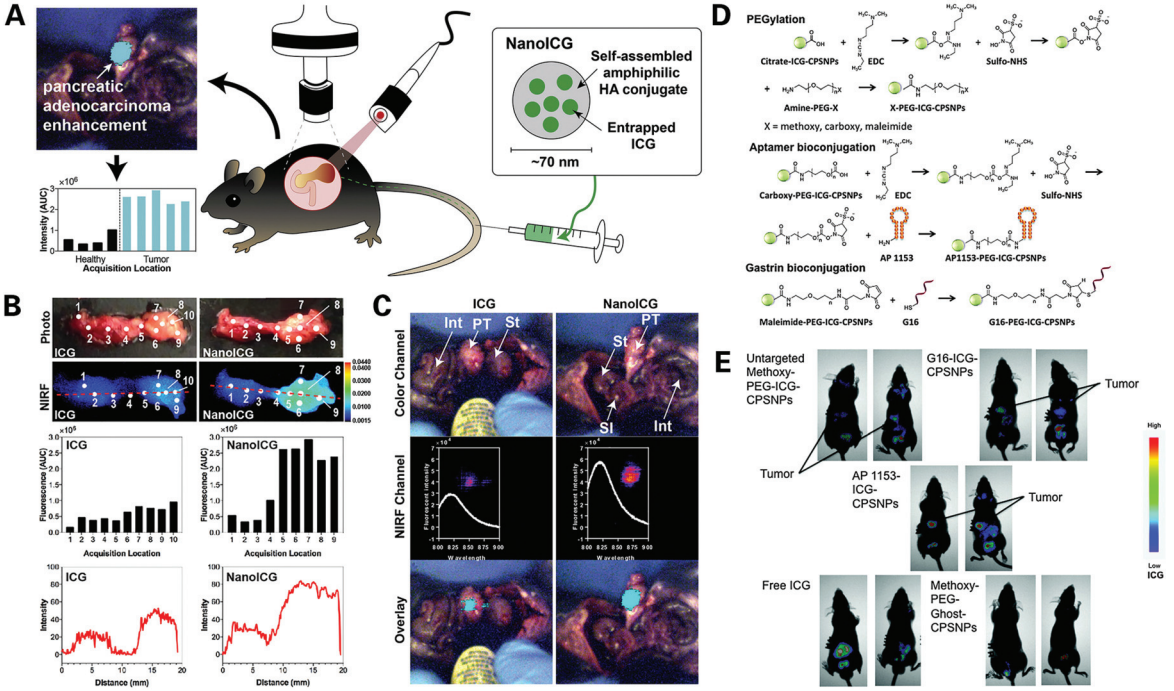

Fig. 3 Novel ICG dye synthesized nanoprobes for the optical imaging of PDAC: (A) illustration of the structure and characterization of the NanoICG and general content of the experiment; (B) surgical navigation images of pancreatic tumor contrast-enhanced with ICG (left) or NanoICG (right) 24 h post intravascular injection, with NanoICG displaying a stronger signal; (C) *ex vivo* assessment of ICG and NanoICG accumulation in pancreatic tumor *via* photo images, NIRF images, analysis of the fluorescence intensity excited with medium laser power, and plots of NIRF image intensity values along the red dashed line. Reproduced with permission from ref. 83. Copyright 2018. Elsevier; (D) synthesis of targeted AP1153–ICG–CPSNPs; (E) assessment of CPSNP uptake by PANC-1 orthotopic tumors *in vivo via* whole-body NIR imaging 15 h post intravascular injection, regarding AP1153–ICG–CPSNPs, unloaded empty particles (methoxy–PEG–GHOST–CPSNPs), or free ICG. Reproduced with permission from ref. 86. Copyright 2017. Mary Ann Liebert.

solve intracellularly, making it a fine vehicle for carrying imaging probes and target ligands. Clawson *et al.* designed a novel nanoprobe termed AP1153-ICG-CPSNPs using CPSNPs doped with ICG and coupled with AP1153, a type of DNA aptamer (AP) that binds to and describes the characterization and targeting efficacy of the G-protein-coupled cholecystokinin B receptor (CCKBR), which is constitutively expressed in PDAC[86] (Fig. 3D). The novel AP1153-ICG-CPSNPs were assessed *in vivo* showing enhanced cellular uptake of this nanoparticle in tumor cells compared to non-targeted ICGs and no uptake in the brain. The particles demonstrated high PDAC-selectivity, and therefore hold promise for the achievement of identifying precursor lesions and early pancreatic lesions before they progress to full-blown PDAC, as well as improving the chemotherapeutic treatments for PDAC patients, so as to improve the patient prognosis.

Albumin has attracted much attention as a carrier for nanoprobe integration.[87,88] Human serum albumin (HSA) is a protein synthesized by the liver, consists of 585 amino acids, and is the most abundant protein in human blood plasma. HSA is widely used in the biotechnology industry, due to its characteristics of non-toxicity, non-immunogenicity and long blood circulation time.[89] HSA contains several hydrophobic binding pockets, making it an ideal transporter for conjugating imaging probes and targeting ligands. Han *et al.* developed a novel enzyme-sensitive albumin-based gemcitabine (GEM) delivery nanoplatform termed HAS-GEM/IR780, by conjugating GEM to HSA, a safe natural carrier, and then complexing it with NIR dye IR780[90] (Fig. 4). The performance of the HAS-GEM/IR780 complex was tested *in vitro* and *in vivo*, and showed an enhanced accumulation and long-term retention over 72 hours compared to free IR780, along with superior tumor inhibition activity compared to free GEM, indicating that HAS-GEM/IR780 serves as a promising agent for the early detection and practical treatment of pancreatic tumors.

Mesoporous nanomaterial with its high specific surface, unique pores volume and size is another novel material drawing great interest in diverse application fields including catalysis, drug delivery and imaging.[91,92] Mesoporous silica is a recent development in nanotechnology, and as a mesoporous form of silica, it exhibits greater loading capacity, is easy to prepare and shows controllable particle and pore size.[93,94] Mesoporous silica nanoparticles (MSN NPs) can be modified to attach imaging probes and targeting ligands, making it a great vehicle for imaging agent synthesis. Li *et al.* designed a novel biodegradable mesoporous silica nanoparticle under 100 nm in diameter termed bMSN@Cy7.5-FA NP as an imaging agent for the detection and quantification of tumor

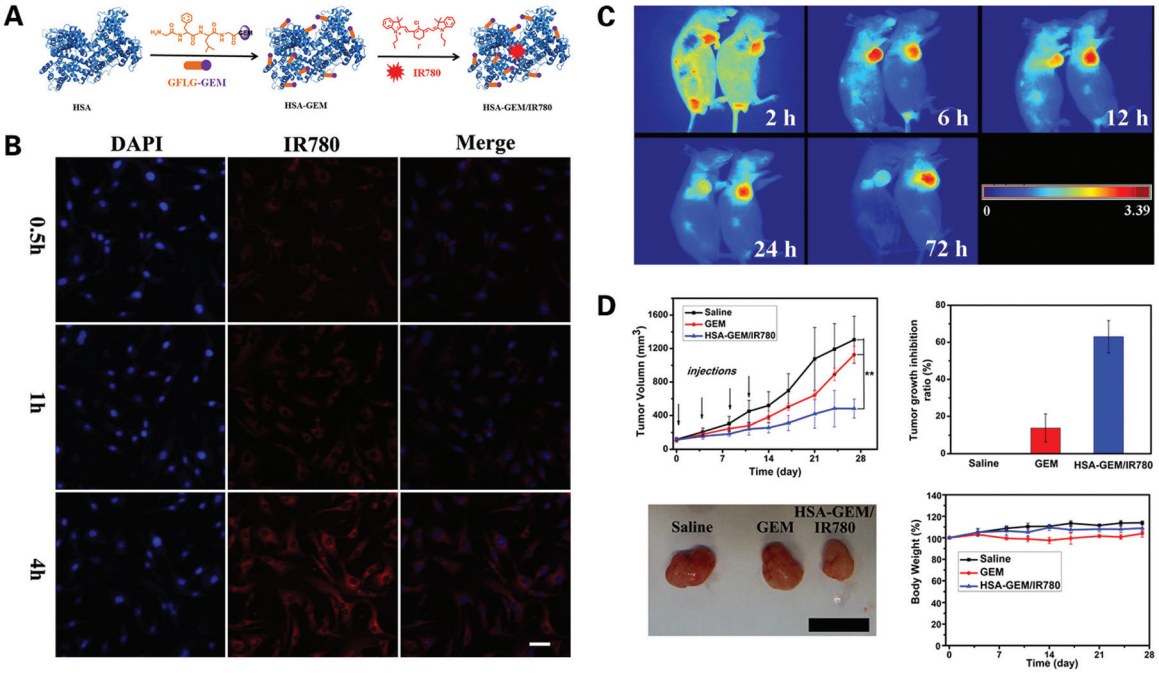

Fig. 4 Novel IR780 dye synthesized nanoprobe for the optical imaging of PDAC: (A) synthesis of HAS–GEM/IR780 complex; (B) assessment of HAS–GEM/IR780 *in vitro via* confocal imaging for 0.5 h, 1 h and 4 h post incubation; (C) assessment of HAS–GEM/IR780 *in vivo via* NIR imaging post injection of free IR780 (left) and HAS–GEM/780 (right); (D) analysis of tumor growth in mice treated with saline, GEM, and HAS–GEM/IR780, respectively, with a scale bar of 2 cm. Reproduced with permission from ref. 90. Copyright 2017. Elsevier.

metastasis, by conjugating cyanine 7.5 NHS ester (Cy7.5) and folic acid (FA), a common target ligand that can selectively bind to folate receptors (FRs) overexpressed on the surface of tumor cells[95] (Fig. 5). These new bMSN@Cy7.5-FA NPs were tested *in vitro* showing no toxicity, good biocompatibility and great targeted cellular uptake, accumulating in the cytoplasm of tumor cells. Then, the *in vivo* experiments showed significantly higher fluorescence intensity compared to non-targeted Cy7.5, with a strong signal intensity even after 12 h, indicating that bMSN@Cy7.5-FA NPs had good stability and excellent potential as agents for carrying out the early detection of PDAC.

2.2.2. Magnetic resonance imaging. MRI measures the concentration and relaxation rate of hydrogen atoms in a strong magnetic field, by employing contrast agents to accelerate the relaxation rate of water molecules, the contrast between specific tissues or organs is increased, thereby improving the imaging sensitivity.[96,97] Magnetic resonance contrast agents are generally classified into two categories based on their relaxation mechanism: T_1-weighted (longitudinal relaxation) contrast agents, mainly including gadolinium (Gd^{3+}) and manganese (Mn^{2+}) NPs, which can display bright signals and fine anatomical structures due to their paramagnetic nature that can increase the T_1 relaxation time; and T_2-weighted (transverse relaxation) contrast agents, mainly including superparamagnetic iron oxide nanoparticles (SPIONPs), which are superparamagnetic materials that reduce the T_2 relaxation time and produce dark signals.[98,99] A sensitive and effective contrast medium is vital for the accurate diagnosis of PDAC by magnetic resonance imaging. The basic requirements of ideal contrast agents for magnetic resonance imaging include appropriate particle size, narrow particle size distribution, excellent magnetic properties, mild toxicity and good compatibility.[100,101] Traditional contrast agents each have their own limitations, for instance, Gd^{3+} based T_1 complexes have the possibility of causing fatal nephrogenic systematic fibrosis (NSF) and metabolism difficulty, while iron oxide nanoparticle-based T_2 contrast agents are less sensitive due to the background interference.[102] Moreover, it is generally difficult for a contrast medium used in MRI scanning to enter PDAC tissue *via* the EPR effect. Fortunately, advances in nanoscience have led to the development of novel nanomaterials applied as MRI contrast agents, which offer advantages including higher biostability and tuneable biodistribution achieved by surface modification; identification of selected targets by conjugation with specific biological molecules, such as antibodies, nucleic acids and peptides; and adjustable imaging properties through changes in the chemical composition, shape and size.[103] In the past five years, novel nanoparticle-based contrast agents for MRI have been gradually applied for the early diagnosis of PDAC in pre-clinic research.[104] Recent progress in MRI nanoparticle-based contrast agents used in the early diagnosis of PDAC will be elaborated in the following contents.

Wang *et al.* designed a dendrimer-based gene-free loading vector with a mean diameter of 110.9 nm, using third-generation dendrigraft poly-L-lysine (DGL) as a nanocarrier scaffold and modified it with gadolinium (Gd), a common type of T_1-weighted contrast agent, and cell-penetrating peptides (CPPs),

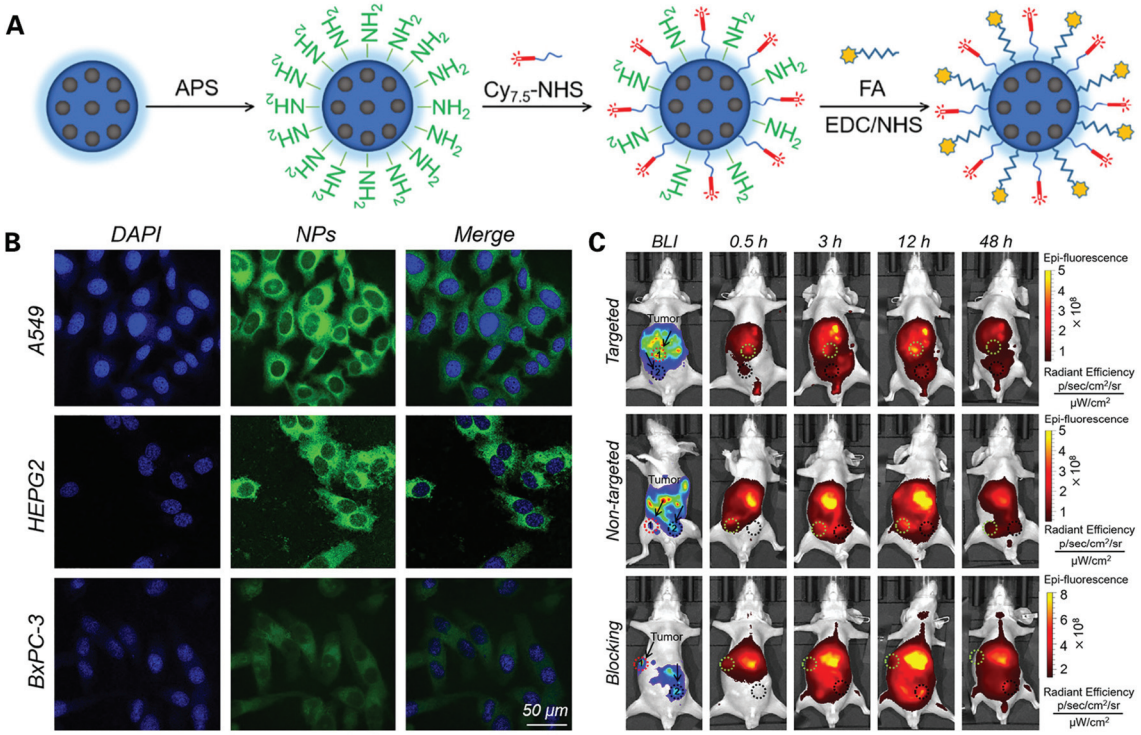

Fig. 5 Novel Cy7.5 dye synthesized nanoprobe for optical imaging of PDAC: (A) construction of bMSN@Cy7.5–FA NPs; (B) assessment of bMSN@Cy7.5–FA NPs *in vitro via* confocal FI in different pancreatic cancer cell lines; (C) assessment of bMSN@Cy7.5–FA NPs *in vivo via* bioluminescence imaging and fluorescence imaging after 48 hours. Reproduced with permission from ref. 95. Copyright 2018. Elsevier.

which are short 30-residue synthetic peptides that can enhance the diffusion of agents through cells, thereby facilitating the cellular uptake of nanoparticles administered regionally in the tumor microenvironment[105] (Fig. 6). Cellular uptake and loaded gene expression of the novel vector were assessed *in vitro*, and the permeability of the vector in tumor stroma and the distribution of transfected gene expression were evaluated *in vivo*. The novel nanoparticle displayed luciferases strictly expressed in the pancreatic tumor region, with higher luminescence intensity and permeability compared with unmodified Gd-based contrast agents, verifying the ability of the novel vector to successfully target and deliver loaded particles to the selected tumor region, while limiting its expression in the targeted tumor tissue, showing great potential in the application of the early and accurate diagnosis of PDAC, as well as guidance in PDAC treatment and tumor change monitoring in patient follow up.

However, Gd-based contrast agents have the disadvantages of potential toxicity, especially the risk of causing fatal nephrogenic systematic fibrosis (NSF) and metabolism difficulty.[103] Iron oxide nanoparticle based T_2 contrast agents have the advantages of non-nephrotoxicity and avoiding the risk of NSF[101] (Fig. 7). He *et al.* designed a biomarker-targeted nanoparticle-based contrast agent termed CXCR4–USPIO for pancreatic cancer cell specific magnetic resonance imaging.[106] The complex was produced by bioconjugating ultrasmall superparamagnetic iron oxide (USPIO) nanoparticles used in magnetic resonance imaging of pancreatic tissue for its ability to offer a significant contrast-enhancement effect, with chemokine receptor 4 (CXCR4) monoclonal antibody, a receptor which has been found to be highly expressed in pancreatic cancer cell lines and primary pancreatic tumors but not in normal pancreatic tissues. The complex was assessed compared to BSA (bovine serum albumin)–USPIO and USPIO. They found a strong correlation between the T_2 enhancement ratio in the CXCR4–USPIO group and the CXCR4 protein expression levels (peptide relative Frey values and mean fluorescence signal intensity) in four different pancreatic cancer cell lines, indicating that the T_2 enhancement ratio of CXCR4–USPIO nanoparticles could be used to semi-quantitatively assess CXCR4 expression levels in cells, showing great potential to achieve PDAC diagnosis at the cellular level.

Later, Mahajan *et al.* designed a complex termed siPLK1–StAv–SPION, by coupling superparamagnetic iron oxide nanoparticles (SPIONs) with polo-like kinase-1 (siOLK1), a siRNA directed against the cell cycle-specific serine–threonine–kinase[107] (Fig. 7A–C). The complex was designed not only to assess targeted delivery efficiency *in vivo* by tumor imaging, but can also serve the purpose of PDAC therapy by delivery of siPLK1, and therefore can be applied to the early diagnosis, treatment and therapeutic effect observation of PDAC. The complex was assessed *in vivo* and showed significant accumulation of siPLK1–StAv–SPIONs in PDAC and inhibition of tumor growth due to silencing of polo-like kinase 1 (PLK1), a

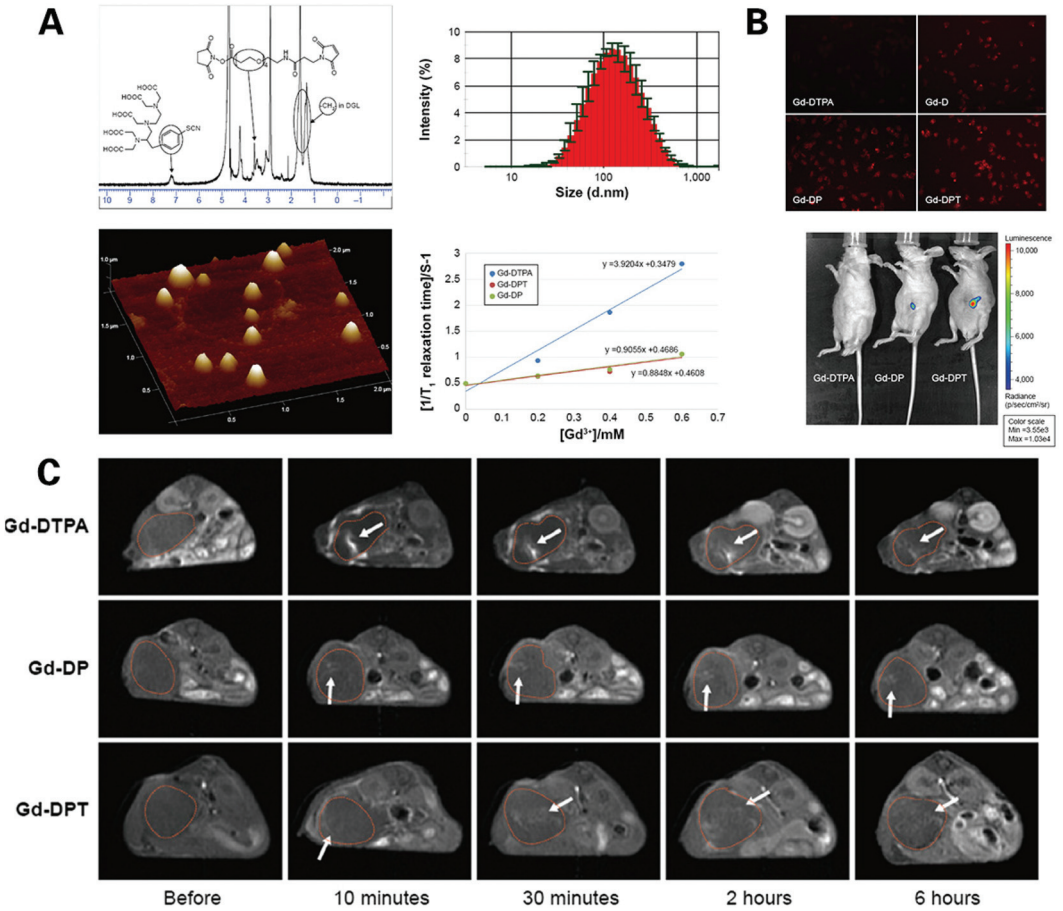

Fig. 6 Gadolinium based nanoprobes for MR imaging of PDAC: (A) characteristics of Gd–DPT/pRFP; (B) assessment of gene transfection *in vitro* and *in vivo via* FI of Gd–DTPA/pRFP (Gd–DTPA), Gd–DGL/pRFP (Gd–D), Gd–DP/pRFP (Gd–DP), and Gd–DPT/pRFP (Gd–DPT); (C) real-time T_1 weighted MR imaging of Gd–DPT/pRFP (Gd–DTPA), Gd–DP/pRFP (Gd–DPT/pDPT) diffusion *in vivo*. Reproduced with permission from ref. 105. Copyright 2015. Dove Press.

proto-oncogene overexpressed in tumor cells, verifying the PDAC targeting function and therapeutic effectiveness of siPLK1–StAv–SPIONs.

Furthermore, Wang *et al.* designed a novel SPIO nanoparticle (30 nm in diameter) targeting Enolase 1 (ENO1) that is a glycolytic enzyme located on the PDAC cell membrane involved in the development, invasion, metastasis and chemoresistance of PDAC, by coupling poly(epsilon-caprolactone)-grafted dextran (Dex-*g*-PCL)/SPIO nanoparticles with the ENO1 antibody[108] (Fig. 7D–F). The tumor detection efficacy of the nanoparticle was tested, showing a stronger signal enhancement of the MRI signal after treatment of ENO1–SPIO compared to SPIO *in vitro* and *in vivo*. A signal enhancement was still overserved 24 h after ENO1–SPIO injection, while the MRI signal intensity was fully recovered to the pre-injection level at 24 h after SPIO injection. These findings indicated that the nanoparticles had satisfactory superparamagnetism and the ability to significantly enhance the detection of PDAC by MRI *in vitro* and *in vivo*, greatly increasing the efficiency of PDAC detection and bringing hope to achieving a higher early diagnosis rate of PDAC.

Moreover, Zou *et al.* generated a novel microminiature nanocomposite of only 23.6 nm diameter termed IONPs–PEG–MCC triple scAbs, by conjugating triple single chain antibodies (scAbs) including scAbMUC4, scAbCEACAM6, scFvCD44v6 and MCC triple scAbs to the surface of polyethylene glycol modified IONPs (IONPs–PEG).[109] IONPs–PEG–MCC triple scAbs as a bi-functional nanocomposite could be used as a negative MR contrast agent for the early and precise diagnosis of PDAC, as well as play a helpful role in PDAC treatment. Magnetic iron oxide nanoparticles (IONPs) are ultrasmall superior contrast agents used in magnetic resonance imaging that can be passively retained in pancreatic tumors due to the EPR effect, as well as be modified to specifically target tumors by artificially attaching tumor-associated biomarkers to its surface. Moreover, instead of attaching a single biomarker, a combination of three biomarkers MUC4, CEACAM6 and CD44v6, all proven in research studies to be potential in the imaging and treatment of pancreatic cancer, was used to promote the sensitivity of PDAC detection and diagnosis. The imaging performance and anti-pancreatic cancer effect of the nanocomposite were evaluated, displaying

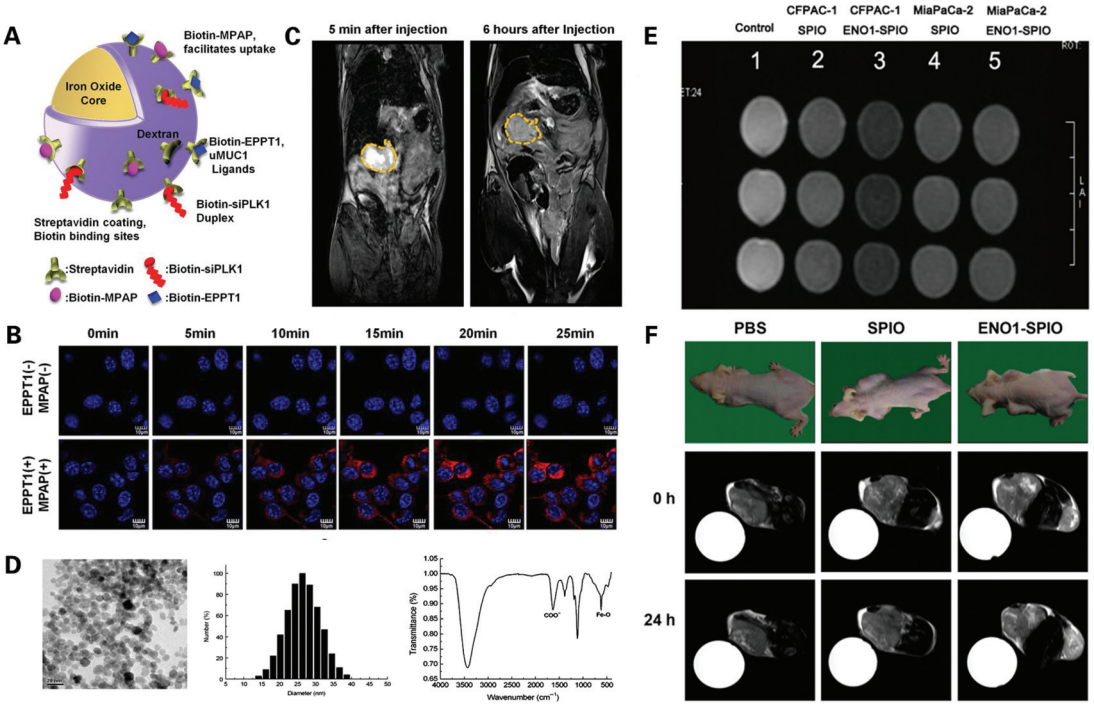

Fig. 7 Iron oxide nanoparticle based nanoprobes for the MR imaging of PDAC: (A) schematic structure of siPLK1–StAv–SPION conjugated to MPAP, EPPT1 and siPLK1; (B) assessment of accumulation of siPLK1–StAv–SPION coupled with or without EPPT1 and MPAP, respectively, *in vitro via* confocal FI over 25 min; (C) assessment of siPLK1–StAv–SPION *in vivo via* MRI pre and 6 h post injection. Reproduced with permission from ref. 107. Copyright 2016. BMJ; (D) characteristics of ENO1-Dex-*g*-PCL/SPIO nanoparticles; (E) assessment of ENO1-Dex-*g*-PCL/SPIO nanoparticles *in vitro via* MRI; (F) assessment of ENO1-Dex-*g*-PCL/SPIO nanoparticles *in vivo via* MRI. Reproduced with permission from ref. 108. Copyright 2020. Wiley.

a decreased T_2-weighted signal intensity of the tumor region of interest (tROI) after injection of modified IONPs compared to non-modified IONPs, and with the increase of scAbs modified to IONPs, the T_2 signal intensity of tROI was decreased to a greater level. Notably, while non-modified IONPs were found to be obviously gathered in the spleen, the modified IONPs gathered specifically in tumor regions. The IONPs–PEG–MCC triple scAbs also exhibited the ability to significantly inhibit tumor growth. These findings confirmed IONPs–PEG–MCC triple scAbs as an excellent dual-functional nanocomposite that can be used in both the diagnosis and treatment of PDAC.

2.2.3. CT imaging. CT is one of the most widely used non-invasive imaging modalities in the clinic, and despite concerns about ionizing radiation, CT continues to play an important role in PDAC diagnosis, often playing the initial imaging method used in detecting PDAC in suspected patients.[27,32] Though CT has a much higher contrast resolution compared to conventional radiography, it is still difficult to distinguish subtle differences of the soft tissue due to the narrow range of CT numbers, and it is difficult to detect microtumors smaller than 1 cm in diameter. CT contrast agents can better delineate regions of interest, and help distinguish healthy tissue and tumor lesions. Approximately half of CT scans are performed using contrast agents.[110] Iodinated molecules and barium sulfate suspensions are widely used, clinically approved contrast agents for X-ray based imaging methods, however, these traditional contrast agents show extremely short blood circulation half-time and patients need to receive a considerable amount of contrast agents due to the low X-ray attenuation coefficient of iodine, increasing the risk of adverse effects including renal insufficiency.[111] Thus, CT contrast agents with better biocompatibility and higher X-ray attenuation coefficients are in great demand for the early detection of PDAC. In the past decade, increasing attention has been paid to the development of nanoparticles as X-ray contrast agents.[112]

Earlier reports of nanomaterials for X-ray contrast agents were mainly based on emulsions or liposomes, and nowadays, more extensive nanoparticle imaging agents based on X-ray contrasting elements including gold, silver, tantalum, bismuth, lanthanides, *etc*. have emerged.[113,114] Nanomaterials also give us synthetic control over size, shape, and composition, which can be designed for various biomedical applications. They also have the advantage of higher payloads per entity, resulting in fewer amounts of contrast agents needed in patients, lowering the renal toxicity and providing more compatibility for patients with impaired kidney function. X-ray nanoparticle agents are generally composed of a contrast generating core coated by compounds that can provide desired pharmacological or physicochemical properties including silica, proteins, polymers, lipids, *etc*.[113] For metal core-based nanoparticle agents, gold has received extensive attention for its high K-edge energy, low density and high biocompatibility.[115,116] Moreover, gold core-based nanoparticles have exhibited a high uptake rate in PDAC cells,

showing potential as a promising candidate for CT imaging of PDAC. Currently, CT is still commonly used in PDAC detection, and therefore the development of nanoparticle contrast agents targeting PDAC for CT imaging can greatly enhance the specificity and sensitivity for the early diagnosis of PDAC.

2.2.4. US/EUS imaging. Among various imaging methods used in the detection of PDAC, US shows the advantages of cost effectiveness and the ability to provide real-time imaging, making it one of the most commonly used imaging modalities in PDAC diagnosis. However, the US imaging quality is often affected by bowel gas, and both US and EUS are highly dependent on the operator experience and patient cooperation.[8,117] Contrast agents can be used to enhance US imaging sensitivity, especially in detecting tumors with poorly organized vessels and microtumors.[118]

Contrast agents are commonly used in other imaging modalities, but contrast agents for US imaging have long been lacking.[119,120] Many novel microbubble ultrasound contrast agents (UCAs) have emerged in the past decade filling out this vacancy and have been approved recently for abdominal mass characterization. Microbubble US contrast agents are mainly composed of an outer shell of a lipid, albumin, or other desirable material, containing a gas core, greatly increasing the blood circulation time and reducing the risk of coalescence, and unlike CT and MR contrast agents, microbubble contrast agents are not filtered by the kidneys with no renal toxicity and do not extravasate into interstitial space. The shell material is ultimately metabolized by the liver and the gas contained is exhaled after bubble dissolution.[121] This novel contrast agent can be modified to target PDAC cells specifically or be used as drug-encapsulating vehicles, to provide sensitive real-time imaging or targeted therapy for PDAC, leading to a precise and early detection of PDAC and a better treatment effect for PDAC patients.

3. Multimodality imaging in the diagnosis of PDAC

Although there are various imaging techniques for the detection of PDAC, all of them have their own advantages as well as limitations. Therefore, at present, single use of any one imaging method alone cannot yet achieve an early and accurate diagnosis of PDAC. Therefore, it is of great significance to develop a new strategy of integrating 2–3 imaging methods into one imaging system, termed multimodal imaging, which can combine the complementary advantages of different imaging modalities.[122,123] Herein, we mainly summarize and discuss the recent advances of multimodality imaging in the early diagnosis of PDAC.

3.1. Magneto-optical nanoplatform for the multimodality imaging of PDAC

Both optical imaging and magnetic resonance imaging have their own advantages and limitations. Optical imaging offers a wide spectrum and deep tissue penetration, but has low spatial resolution and cannot obtain comprehensive three-dimensional anatomical structure images.[38,68] Also, PAI displays the disadvantage of not being able to image through bones or air-filled structures, and there is no mature commercial PDAC PAI system available yet.[124] Thus, the clinical application of PAI in the early diagnosis of PDAC is still under exploration. As for MRI, although it is non-invasive and has no use of ionizing radiation, MRI is expensive, has low sensitivity, cannot obtain real-time imaging and may be uncomfortable for patients with claustrophobia due to its long examination time and narrow exam space.[36] In addition, though the development and application of signal enhancing contrast agents have provided improvement of the specificity and sensitivity of MRI to a certain extent, the contrast agents themselves also have many problems yet to be solved. Gd^{3+} based T_1 contrast agents are nephrotoxic, SPIONPs based T_2 contrast agents have great imaging performance and low nephrotoxicity, but has low stability *in vivo* and may cause serious DNA and protein damage, even systemic inflammatory due to the production of reactive oxygen species (ROS).[98,103,107] The use of magneto-optical nanoplatform is a novel multimodality imaging method combining optical imaging and MRI, so as to produce the complementary effect. Multimodal imaging nanoparticles are generally a complex of optical luminescent dyes and MRI contrast agents, which can be applied to optical imaging and MRI imaging at the same time, and when the nanoparticles can generate the photothermal effect, they can also be used in photoacoustic imaging.[125,126] In this case, not only can these nanoparticles specifically provide PDAC targeted comprehensive three-dimensional anatomical images of pancreatic tumors, but can also obtain real-time visual information of the tumors.[127,128] Recent advances in the magneto-optical nanoplatform for the multimodality imaging of PDAC will be elaborated in the following contents (Fig. 8).

MR contrast agents can be conjugated with fluorescence imaging agents to provide complementary imaging of PDAC. Gd-based materials are commonly used in modifying MR-fluorescent agents, by conjugating them with fluorescent dyes and targeting ligands. Wang *et al.* designed a novel bispecific molecular probe termed Gd–Cy7–PTP/RGD aimed to be used for both MRI and NIRF of pancreatic cancer[129] (Fig. 8A and B). The novel bispecific molecular probe was synthesized by conjugating Gd, a common T_1-weighted contrast agent, cyanine 7 (Cy7), a common NIRF dye, the peptide PTP that binds to plectin-1 which is specifically overexpressed on the surface of PDAC cells, and the peptide RGD that targets integrin widely expressed on pancreatic duct epithelial cells and angiogenesis in malignant tumors. The bispecific probes were evaluated *in vitro* and *in vivo* and showed that the combination of PTP and RGD modified probes provided a great increase in the targeting efficiency of PDAC *in vitro* and *in vivo* compared to non-modified agents and agents modified with a single peptide. The bispecific probes not only target pancreatic neoplasms but also target angiogenesis in tumors at the same time, thereby producing a multi-level targeting effect. NIRF-guided intraoperative delineation of surgical margins and tumor excision

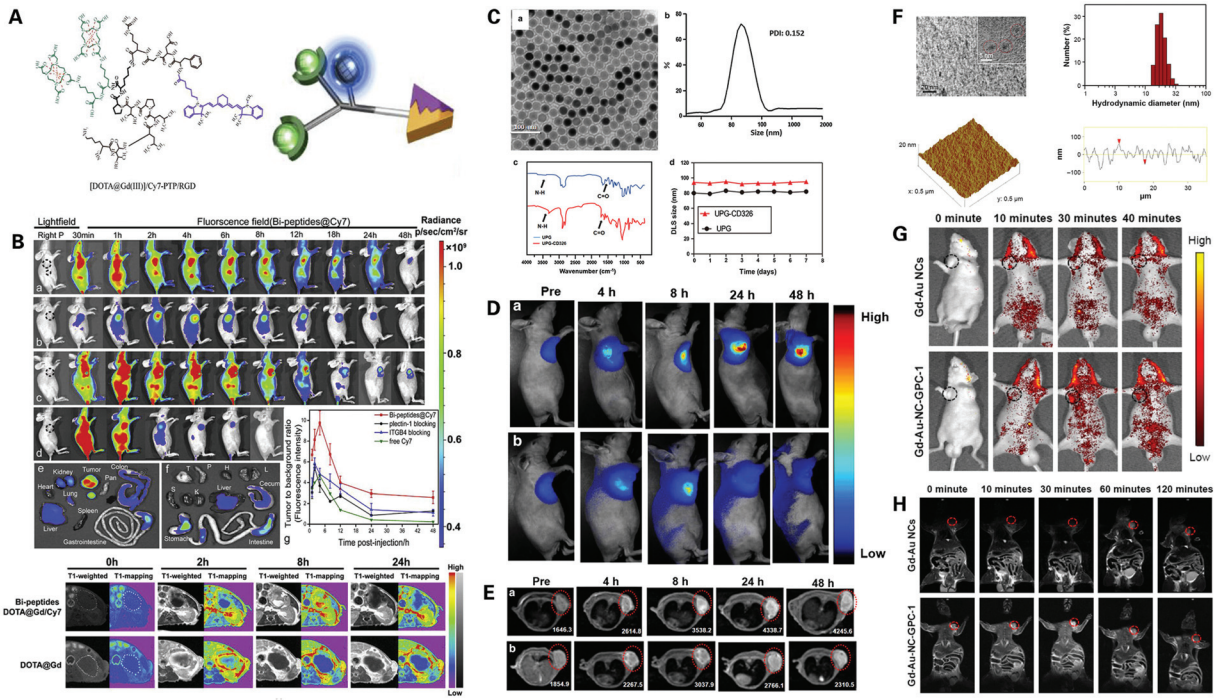

Fig. 8 Magneto-optical nanoplatform for the multimodality imaging of PDAC: (A) schematic structure of Gd–Cy7–PTP/RGD; (B) bio-distribution and assessment of Gd–Cy7–PTP/RGD (a) *in vivo via* dual-modality imaging, compared with plectin-1 McAb (b), ITGB4 McAb blocking (c) and free Cy7 (d). Reproduced with permission from ref. 129. Copyright 2018. Elsevier; (C) characteristics of UPG–CD326 micelles; assessment of UPG–CD326 micelles (a) *in vivo via* real-time upconversion luminescence imaging (D) and real-time T_1-weighted MRI (E) compared with non-targeted UPG (b). Reproduced with permission from ref. 131. Copyright 2018. BMC; (F) characteristics of Gd–Au–NC–GPC-1; assessment of Gd–Au–NC–GPC-1 *in vivo via* real-time FI (G) and real-time MRI (H) compared with Gd–Au NCs. Reproduced with permission from ref. 132. Copyright 2018. Dove Press.

was achieved *in vivo* under the navigation of MR/NIRF bimodality imaging, which provided high spatial resolution, high sensitivity, high specificity and real-time visualization simultaneously, promoting further exploration and development of multi-specific probes for the early diagnosis and treatment guidance of PDAC.

Later, Li *et al.* designed a dual-modal imaging nanoprobe termed dendron-grafted polylysine (DGL–U11), by using third generation dendron G3 of DGL (DGL–G3) as the platform, due to its desirable properties of good biocompatibility, biodegradability, distinct sizes, *etc.*[130] to load U11, a peptide targeting receptor uPAR overexpressed in pancreatic tumors, Gd^{3+}-diethylenetriamine pentaacetic acid, a T_1-weighted contrast agent, and Cy5.5, a NIRF imaging dye. The nanoprobe was assessed *in vitro* and *in vivo* showing a significantly higher fluorescence intensity in DGL–U11 nanoparticle incubated tumor cells compared to non-targeted agents, and an increasingly enhanced MR signal and fluorescence signal in different tumor stages compared to non-targeted control. The above findings confirm that this novel uPAR-targeted dual-modal nanoprobe serves as an excellent contrast agent in the targeted imaging of precancerous PanINs and PDAC lesions in both MR and NIRF imaging simultaneously, providing both high sensitivity and high spatial resolution, bringing great hope to the early diagnosis of PDAC.

Furthermore, Han *et al.* designed a novel micelle probe termed UPG–CD326, by synthesizing gadolinium ion-doped upconversion nanoparticles (UCNPs) that can be used in magnetic resonance imaging and fluorescence imaging simultaneously, with anti-human CD326 monoclonal antibody targeting CD326, a transmembrane glycoprotein overexpressed on pancreatic cancer stem cells[131] (Fig. 8C–E). The micelles were assessed *in vitro* and *in vivo* and exhibited superior imaging properties, long-time stability and good biocompatibility, showing a higher fluorescence and MR signal intensity compared to non-targeted agents, indicating a significant enhancement of the cellular uptake of micelles through a CD326 antigen–antibody mediated endocytosis process, exhibiting both passive and active CD326 targeting abilities of the targeted micelles, even after 48 h, while non-targeted micelles only showed passive tumor targeting ability *via* the EPR effect, verifying the excellent targeting function of UPG–CD326 micelles. These findings demonstrated great potential for achieving an early and accurate diagnosis of PDAC in the future.

Moreover, Huang *et al.* designed a dual-modal imaging probe termed NCs; Gd–Au–NC–GPC-1 by conjugating Gd–Au nanoclusters with Glypica-1 (GPC-1) antibody targeting GPC-1, a type of cell surface heparan sulfate proteoglycan highly expressed in pancreatic cancer cells[132] (Fig. 8F–H). The probe

was assessed *in vitro* and *in vivo*, displaying an enhanced MR and fluorescent signal compared to non-targeted probes, suggesting that Gd–Au–NC–GPC-1 can target pancreatic cancer cells selectively in both fluorescence imaging and MR imaging. FI displayed high sensitivity but could only provide whether Gd–Au–NC–GPC-1 was targeted to the tumor and give an approximate position *in vivo*, however, this limitation was remedied *via* MR imaging which could clearly demonstrate the exact location of the tumor. Therefore, this novel dual-modal FI/MRI probe showed great potential in the application of early diagnosis of PDAC.

Iron oxide nanoparticles can be easily synthesized with a fluorescent dye and targeting ligand, making it a popular choice for the MR-fluorescencet imaging of PDAC. Medina *et al.* designed a novel nanoparticle by encapsulating iron nanoparticles and ICG into cationic sphingomyelin (SM) consisting of liposomes that had an RA-96 Fab fragment conjugated on its surface in order to increase the tumor homing ability.[133] The targeting ability and MRI photoacoustic visibility of RA-96-targeted liposomes encapsulating iron nanoparticles and ICG were tested *in vitro* and *in vivo* exhibiting increased association of ICG-encapsulated liposomes coated with RA-96 Fab fragments *in vitro* compared to non-targeted agents in FI, and increased accumulation of RA-96-targeted nanoparticles in tumor sites compared to non-targeted controls *in vivo via* FI and MRI, indicating that RA-96-targeted iron nanoparticles and ICG-encapsulated liposomes can be applied to imaging pancreatic tumors using a variety of optical and magnetic imaging techniques or even be suitable for drug delivery in PDAC treatment.

Furthermore, Wang *et al.* designed a novel dual-modality molecular imaging contrast agent termed MN–EPPT, by conjugating dextran-coated iron oxide nanoparticles to NIRF dye Cy5.5 and a peptide EPPT targeting uMUCI, an overexpressed and underglycosylated biomarker on over half of human cancers.[134] The novel contrast agent was tested *in vitro* and *in vivo*, showing a significantly reduced accumulation of MN–EPPT, as to a lower level of uMUCI expression in both MRI and optical imaging in the treatment group using gemcitabine as chemotherapy compared to the saline control. Histopathological results confirmed the findings above showing a normal prevalent glandular structure in the gemcitabine group and high-grade PanIN lesions and CIS in the saline control group. This novel contrast agent showed great potential in the early diagnosis and evaluation of treatment assessment of PDAC.

3.2. Other multi-modality imaging of PDAC

At present, multimodal imaging nanoparticles are generally a combination of optical luminescent dyes and MRI contrast agents, but agents of other imaging modalities commonly used in the diagnosis of PDAC can also be integrated to synergistically provide more accurate imaging of PDAC, contributing to earlier and more accurate diagnosis, guidance in surgery and treatment, as well as the assessment of therapeutic outcomes. US and optical imaging can be combined to obtain anatomic, target specific and real-time imaging of PDAC. Barrefelt *et al.* designed a novel nanoprobe termed VivoTag 680 MBs, by labelling air-filled polyvinyl alcohol microbubbles (PVA–MBs), a newly introduced contrast agent for US imaging, with a NIR fluorophore, VivoTag 680.[135] The novel nanoparticle was tested *in vivo via* US imaging showing highly fluorescent signals only in PDAC tumor surrounding tissues but not inside the tumor, which successfully demonstrated the poor vascularization of PDAC, indicating the potential application of PVA–MBs as a multimodal imaging contrast agent for early PDAC diagnosis. PET/CT and EUS may also be combined to complement the high sensitivity of PET/CT and high specificity of EUS.[136]

MR contrast agents can also be conjugated with both optical imaging agents and X-ray contrast agents forming a triple-modality platform to obtain comprehensive imaging of PDAC. Zhao *et al.* designed a core–shell structured gold nanorod (AuNR) to be used as a contrast agent for multimodal imaging applied to the early diagnosis of PDAC[137] (Fig. 9). The nanoparticles are composed of a AuNR core with a mesoporous silica outside layer, which was coated with a gadolinium oxide carbonate shell, and the resulting AuNR–SiO_2–Gd can then be used in MRI, CT and optical imaging. The AuNR–SiO_2–Gd NPs were assessed *in vitro* showing higher MRI contrast compared to Gadovist, higher X-ray attenuation compared to Visipaque, and strong PA contrast enhancement within the examined range of 680–970 nm with a peak absorbance at around 800 nm. The nanoparticles were then tested *in vivo*, showing high accumulation of AuNR–SiO_2–Gd NPs in surrounding tissues but little distribution throughout the tumor caused by dense stoma infiltration and hypovascularity, leading to a negative contrast within the tumor portion in CT/PAI and a positive contrast in MRI. These findings suggest that AuNR–SiO_2–Gd NPs have great potential as a multimodal contrast medium for the early detection of PDAC, hoping to improve early diagnosis and benefit patient outcomes.

Contrast agents of potential imaging modalities for PDAC diagnosis can also be integrated to provide complementary and more accurate imaging of PDAC. MPI, as an emerging imaging modality with great potential in the application of PDAC diagnosis, traces the spatial distribution of magnetic nanoparticle agents and detects the change in iron electronic magnetization, unlike MRI which measures the change in water proton nuclear magnetization, and therefore provides much higher sensitivity than MRI, with nearly zero background signal and zero signal attenuation for analysis of in-depth tissues.[62] Therefore, nanomaterials that can be used in both MPI and optical imaging may show greater advantages in the early detection of cancer compared to current imaging examinations. Though also a magnetic imaging modality, there is a great difference in physics between MPI and MRI, and therefore common MRI contrast materials like iron oxide nanoparticles are not ideal for MPI. Song *et al.* discovered that FeCo nanoparticles that bear a poly(ethylene glycol) decorated graphic carbon shell provide an MPI signal intensity much higher than the signals from SPIONs at the same molar con-

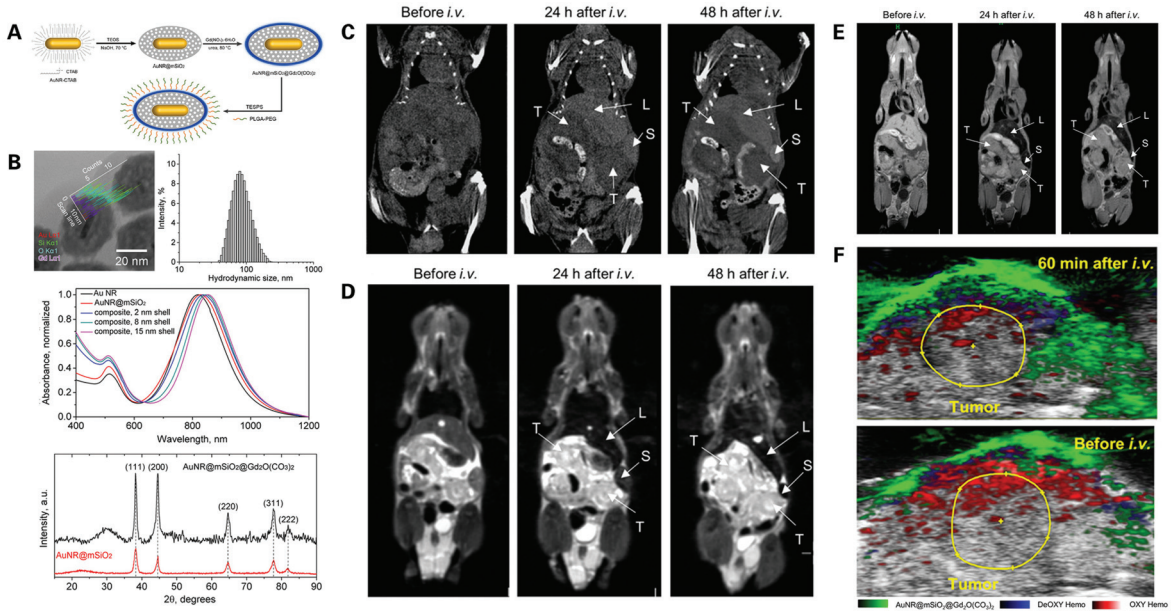

Fig. 9 Nanoprobes for the triple-modality imaging of PDAC: (A) schematic synthesis procedure of AuNR@$mSiO_2$@$Gd_2O(CO_3)_2$ NPs; (B) characteristics of AuNR@$mSiO_2$@$Gd_2O(CO_3)_2$ NPs; assessment of AuNR@$mSiO_2$@$Gd_2O(CO_3)_2$ NPs *in vivo via* whole-body CT imaging (C), T_2-weighted MR imaging (D), T_1-weighted MR imaging (E), and PA imaging (F) at different time periods. Reproduced with permission from ref. 137. Copyright 2020. ACS.

centration of iron[138] (Fig. 10F–K). Notably, the novel nanoparticle was tested and it showed both photothermal and magnetothermal properties, with high optical absorbance in the NIR region (700–1200 nm wavelength), indicating that this nanoparticle is suitable as a tracer in both MPI and optical imaging, showing great potential in the early detection of PDAC after modification adding targeting functions.

MPI contrast nanoparticles can even be modified to be used in MPI, MRI, PAI and FI, combining all complementary advantages of all four imaging modalities, providing a precise and comprehensive assessment of tumor lesions. Song *et al.* designed a novel multimodality nanoparticle termed MMPF NPs for imaging tumor *in vivo via* MPI, MRI, PAI and FI[139] (Fig. 10A–E). The novel nanoparticles were assessed and showed long blood circulation time with a half-life of 49 h, and high tumor uptake. Notably, MMPF NPs offered ultrasensitive real-time imaging of tumors *via* MPI. MMPF NPs have been tested in breast and brain tumors *via* simultaneous MPI, MRI, PAI and FI showing outstanding contrast between tumor lesions and normal tissues, demonstrating great poten-

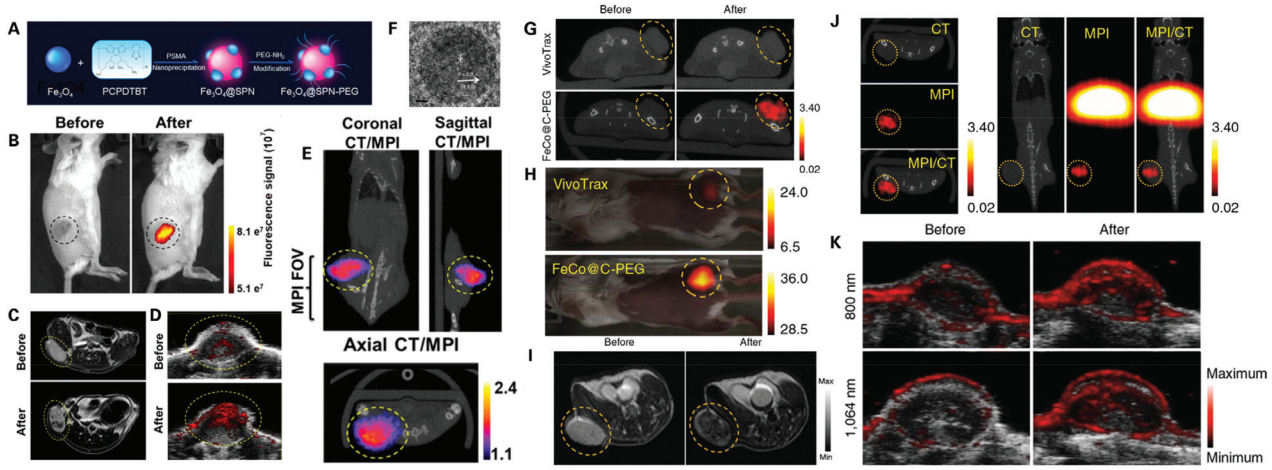

Fig. 10 Potential nanoprobes for the multimodality imaging of PDAC: (A) schematic synthesis of MMPF NPs; assessment of MMPF NPs *in vivo via* FI (B), T_2-MRI (C), PAI (D), and MPI/CT (E). Reproduced with permission from ref. 139. Copyright 2019. ACS; (F) high-resolution TEM image of FeCo@C–PEG; (G and H) assessment of FeCo@CPEG in mice bearing breast tumors *via* MPI/CT compared with VivoTrax; assessment of FeCo@CPEG in mice bearing breast tumors *via* MRI (I), CT, MPI and MPI/CT (J), and PAI (K). Reproduced with permission from ref. 138. Copyright 2020. Nature.

tial in the application of cancer diagnosis. The novel nanoparticle also showed great potential in the early and accurate detection of PDAC after modification with PDAC specific targeting ligands, or even be used to monitor PDAC treatment *via* a desired modification.

PAI is a novel biomedical imaging method and there is no mature commercial PDAC PAI system available yet, and the application of PAI in early diagnosis of PDAC is limited to preclinical studies. However, compared with luminescence imaging, PAI can provide deeper tissue penetration and relatively higher sensitivity, showing great potential in the clinical application of early PDAC diagnosis.[60] By modifying agents that can be used in both magnetic imaging and PAI, the combination of both imaging modalities endow better accuracy and higher penetration depth to lesion visualization. Chen *et al.* designed a nanoprobe based on Prussian blue (PB) which can be used to combine MRI and PAI for deep tissue imaging.[140] The PB nanoparticle was designed to function as an indicator for sensing peroxynitrite ($ONOO^-$), a reactive oxygen species (ROS) in pathological and physiological prosses, to detect drug-induced liver injury. Such a magnetic/photoacoustic nanoplatform for multi-modality imaging can be referred to in the development of novel nanomaterials for multi-modality imaging in the early diagnosis of solid tumors.

4. Conclusion and prospects

This review comprehensively introduced imaging methods for the diagnosis of PDAC and highlighted the current magneto-optical nanoplatform in multimodality imaging for the enhanced early diagnosis of PDAC. We believe that with an in-depth understanding of biological interactions that occur in the unique PDAC microenvironment, it is increasingly important for materials scientists, clinicians, and other researchers to integrate ideas into the development of a novel magneto-optical nanoplatform both preclinically and clinically, especially in the areas of multimodality imaging for achieving an early diagnosis of PDAC. We hope this review can inspire the design and fabrication of nanoprobes in multimodality imaging for achieving an early diagnosis of pancreatic cancer, so as to raise the clinical benefits in PDAC patients.

Although many researchers made a lot of effort to improve the early diagnosis rate of pancreatic cancer *via* the development of multimodality imaging particularly the magneto-optical nanoplatform. Many challenges remain, and we need to explore new strategies to solve the below problems. The specificity of the nanoplatform for distinguishing PDCA cells from normal pancreatic cells is not enough, resulting in excessive interference by background signals. To address this challenge, it is expected to develop an "off–on" switchable nanoplatform with a specific function assisted by a responsive polymer, i-motif DNA, or even a chemical bond, which can selectively turn on the imaging signals triggered by the stimuli in tumor tissues while keeping the imaging signals powered off in normal tissues, so as to further amplify the imaging signal in PDAC tissue and reduce the interference signal of the background, thereby improving the early diagnosis rate of PDCA. Furthermore, patient derived xenotransplantation models or genetically engineered mouse models (GEMMs) are recommended to verify the function of the magneto-optical nanoplatform, so as to promote these nanomedicines from bench to bedside. Moreover, many newly emerged imaging modalities such as MPI and PAI show great potential in the early detection of PDAC, however, the development of novel nanomaterials for these imaging methods in the diagnosis of PDAC is still lacking. Meanwhile, nanoparticle contrast agents for the current commonly used imaging methods such as CT and US are also lacking, appealing more exploration in these fields, to help achieve a higher early and accurate diagnosis rate of PDAC.

Author contributions

X. Z., J. X., and G. S. designed the review, X. Z. wrote the manuscript, Z. Z., L. X., H. L., S. X., J. X. and G. S. edited the paper. J. X. and G. S. revised the paper. All authors gave final approval to the article.

Conflicts of interest

There are no conflicts to declare.

Acknowledgements

This work was supported by the National Natural Science Foundation of China (grants U21A20287, 51872088) and the Science and Technology Project of Hunan Province (2020RC3022; 2020SK2014).

References

1 A. Vincent, J. Herman, R. Schulick, R. H. Hruban and M. Goggins, *Lancet*, 2011, **378**, 607–620.
2 E. Riquelme, Y. Zhang, L. Zhang, M. Montiel, M. Zoltan, W. Dong, P. Quesada, I. Sahin, V. Chandra, A. San Lucas, P. Scheet, H. Xu, S. Hanash, L. Feng, J. Burks, K. Do, C. Peterson, D. Nejman, C. Tzeng, M. Kim, C. Sears, N. Ajami, J. Petrosino, L. Wood, A. Maitra, R. Straussman, M. Katz, J. White, R. Jenq, J. Wargo and F. McAllister, *Cell*, 2019, **178**, 795–806.
3 R. Siegel, K. Miller, H. Fuchs and A. Jemal, *Ca-Cancer J. Clin.*, 2021, **71**, 7–33.
4 H. Sung, J. Ferlay, R. Siegel, M. Laversanne, I. Soerjomataram, A. Jemal and F. Bray, *Ca-Cancer J. Clin.*, 2021, **71**, 209–249.
5 M. Schmidt-Hansen, S. Berendse and W. Hamilton, *Pancreas*, 2016, **45**, 814–818.

6 A. Bengtsson, R. Andersson and D. Ansari, *Sci. Rep.*, 2020, **10**, 16425.
7 T. Schnelldorfer, A. Ware, M. Sarr, T. Smyrk, L. Zhang, R. Qin, R. Gullerud, J. Donohue, D. Nagorney and M. Farnell, *Ann. Surg.*, 2008, **247**, 456–462.
8 L. Zhang, S. Sanagapalli and A. Stoita, *World J. Gastroenterol.*, 2018, **24**, 2047–2060.
9 A. Singhi, E. Koay, S. Chari and A. Maitra, *Gastroenterology*, 2019, **156**, 2024–2040.
10 L. Zhang, S. Sanagapalli and A. Stoita, *World J. Gastroenterol.*, 2018, **24**, 2047–2060.
11 V. Goral, *Asian Pac. J. Cancer Prev.*, 2015, **16**, 5619–5624.
12 D. Marrelli, S. Caruso, C. Pedrazzani, A. Neri, E. Fernandes, M. Marini, E. Pinto and F. Roviello, *Am. J. Surg.*, 2009, **198**, 333–339.
13 S. Su, S. Qin, W. Chen, W. Luo and H. Jiang, *World J. Gastroenterol.*, 2015, **21**, 4323–4333.
14 R. Prokesch, L. Chow, C. Beaulieu, R. Bammer and R. Jeffrey, *Radiology*, 2002, **224**, 764–768.
15 N. Balci and R. Semelka, *Eur. J. Radiol.*, 2001, **38**, 105–112.
16 M. Barral, B. Taouli, B. Guiu, D. M. Koh, A. Luciani, R. Manfredi, V. Vilgrain, C. Hoeffel, M. Kanematsu and P. Soyer, *Radiology*, 2015, **274**, 45–63.
17 S. van Asselt, A. Brouwers, H. van Dullemen, E. van der Jagt, A. Bongaerts, I. Kema, K. Koopmans, G. Valk, H. Timmers, W. de Herder, R. Feelders, P. Fockens, W. Sluiter, E. de Vries and T. Links, *Gastrointest. Endosc.*, 2015, **81**, 159–167.
18 W. Wang, A. Shpaner, S. Krishna, W. Ross, M. Bhutani, E. Tamm, G. Raju, L. Xiao, R. Wolff, J. Fleming and J. Lee, *Gastrointest. Endosc.*, 2013, **78**, 73–80.
19 S. Dougan, *Cancer J.*, 2017, **23**, 321–325.
20 A. Rucki and L. Zheng, *World J. Gastroenterol.*, 2014, **20**, 2237–2246.
21 J. McCarroll, J. Teo, C. Boyer, D. Goldstein, M. Kavallaris and P. Phillips, *Front. Physiol.*, 2014, **5**, 2.
22 W. Tummers, J. Willmann, B. Bonsing, A. Vahrmeijer, S. Gambhir and R. Swijnenburg, *Pancreas*, 2018, **47**, 675–689.
23 D. Shahbazi-Gahrouei, P. Moradi Khaniabadi, B. Moradi Khaniabadi and S. Shahbazi-Gahrouei, *J. Res. Med. Sci.*, 2019, **24**, 38.
24 N. Lamichhane, S. Sharma, Parul, A. K. Verma, I. Roy and T. Sen, *Biomedicines*, 2021, **9**, 288.
25 B. Ren, M. Cui, G. Yang, H. Wang, M. Feng, L. You and Y. Zhao, *Mol. Cancer*, 2018, **17**, 108.
26 D. W. Townsend, *J. Nucl. Med.*, 2008, **49**, 938–955.
27 T. Tamada, K. Ito, N. Kanomata, T. Sone, A. Kanki, A. Higaki, M. Hayashida and A. Yamamoto, *Eur. Radiol.*, 2016, **26**, 646–655.
28 T. Iiboshi, K. Hanada, T. Fukuda, S. Yonehara, T. Sasaki and K. Chayama, *Pancreas*, 2012, **41**, 523–529.
29 W. Wang, A. Shpaner, S. G. Krishna, W. A. Ross, M. S. Bhutani, E. P. Tamm, G. S. Raju, L. Xiao, R. A. Wolff, J. B. Fleming and J. H. Lee, *Gastrointest. Endosc.*, 2013, **78**, 73–80.
30 J. R. Treadwell, H. M. Zafar, M. D. Mitchell, K. Tipton, U. Teitelbaum and J. Jue, *Pancreas*, 2016, **45**, 789–795.
31 L. W. Goldman, *J. Nucl. Med. Technol.*, 2007, **35**, 115–128.
32 K. M. Horton and E. K. Fishman, *Am. J. Roentgenol.*, 2002, **178**, 827–831.
33 I. Matsumoto, S. Shirakawa, M. Shinzeki, S. Asari, T. Goto, T. Ajiki, T. Fukumoto, K. Kitajima and Y. Ku, *Clin. Gastroenterol. Hepatol.*, 2013, **11**, 712–718.
34 K. Okano, K. Kakinoki, S. Akamoto, M. Hagiike, H. Usuki, Y. Yamamoto, Y. Nishiyama and Y. Suzuki, *World J. Gastroenterol.*, 2011, **17**, 231–235.
35 Y. Wang, F. H. Miller, Z. E. Chen, L. Merrick, K. J. Mortele, F. L. Hoff, N. A. Hammond, V. Yaghmai and P. Nikolaidis, *RadioGraphics*, 2011, **31**, E47–E64.
36 V. P. Grover, J. M. Tognarelli, M. M. Crossey, I. J. Cox, S. D. Taylor-Robinson and M. J. McPhail, *J. Clin. Exp. Neuropsychol.*, 2015, **5**, 246–255.
37 C. Wang, Z. Wang, T. Zhao, Y. Li, G. Huang, B. Sumer and J. Gao, *Biomaterials*, 2018, **157**, 62–75.
38 G. Pirovano, S. Roberts, S. Kossatz and T. Reiner, *J. Nucl. Med.*, 2020, **61**, 1419–1427.
39 M. L. James and S. S. Gambhir, *Physiol. Rev.*, 2012, **92**, 897–965.
40 C. Hoogstins, L. Boogerd, B. Sibinga Mulder, J. Mieog, R. Swijnenburg, C. van de Velde, A. Farina Sarasqueta, B. Bonsing, B. Framery, A. Pèlegrin, M. Gutowski, F. Cailler, J. Burggraaf and A. Vahrmeijer, *Ann. Surg. Oncol.*, 2018, **25**, 3350–3357.
41 C. Wang, Z. Wang, T. Zhao, Y. Li, G. Huang, B. D. Sumer and J. Gao, *Biomaterials*, 2018, **157**, 62–75.
42 Y. Peng, B. Xiong, L. Peng, H. Li, Y. He and E. S. Yeung, *Anal. Chem.*, 2015, **87**, 200–215.
43 F. Stuker, J. Ripoll and M. Rudin, *Pharmaceutics*, 2011, **3**, 229–274.
44 M. E. Roth-Konforti, C. R. Bauer and D. Shabat, *Angew. Chem., Int. Ed.*, 2017, **56**, 15633–15638.
45 C. Lu, C. Zhang, P. Wang, Y. Zhao, Y. Yang, Y. Wang, H. Yuan, S. Qu, X. Zhang and G. Song, *Chem*, 2020, **6**, 2314–2334.
46 N. Hananya, A. Eldar Boock, C. R. Bauer, R. Satchi-Fainaro and D. Shabat, *J. Am. Chem. Soc.*, 2016, **138**, 13438–13446.
47 M. Yang, J. Huang, J. Fan, J. Du, K. Pu and X. Peng, *Chem. Soc. Rev.*, 2020, **49**, 6800–6815.
48 B. Wang, Y. Wang, Y. Wang, Y. Zhao and X. B. Zhang, *Anal. Chem.*, 2020, **92**, 4154–4163.
49 Y. Wang, L. Shi, Z. Ye, K. Guan, L. Teng, J. Wu, X. Yin, G. Song and X. Zhang, *Nano Lett.*, 2020, **20**, 176–183.
50 M. Blanco-Formoso and R. Alvarez-Puebla, *Int. J. Mol. Sci.*, 2020, **21**, 2253.
51 T. Moore, A. Moody, T. Payne, G. Sarabia, A. Daniel and B. Sharma, *Biosensors*, 2018, **8**, 46.
52 W. Li and X. Chen, *Nanomedicine*, 2015, **10**, 299–320.
53 J. Glatz, N. Deliolanis, A. Buehler, D. Razansky and V. Ntziachristos, *Opt. Express*, 2011, **19**, 3175–3184.
54 S. Tzoumas and V. Ntziachristos, *Philos. Trans. R. Soc., A*, 2017, **375**, 20170262.

55 W. Zhu, M. Chen, Y. Liu, Y. Tian, Z. Song, G. Song and X. Zhang, *Nanoscale*, 2019, **11**, 20630–20637.
56 B. Yin, Y. Wang, C. Zhang, Y. Zhao, Y. Wang, L. Teng, Y. Yang, Z. Zeng, S. Huan, G. Song and X. Zhang, *Anal. Chem.*, 2019, **91**, 15275–15283.
57 Y. Ma, L. Xu, B. Yin, J. Shang, F. Chen, J. Xu, Z. Song, B. Nan, G. Song and X. Zhang, *Nano Lett.*, 2021, **21**, 4484–4493.
58 Y. Zhou, J. Yao and L. V. Wang, *J. Biomed. Opt.*, 2016, **21**, 61007.
59 Z. Yuan and H. Jiang, *Opt. Lett.*, 2009, **34**, 1714–1716.
60 L. Zeng, G. Ma, J. Lin and P. Huang, *Small*, 2018, **14**, e1800782.
61 J. Haegele, T. Sattel, M. Erbe, K. Luedtke-Buzug, M. Taupitz, J. Borgert, T. Buzug, J. Barkhausen and F. Vogt, *RoeFo, Fortschr. Geb. Roentgenstr. Nuklearmed.*, 2012, **184**, 420–426.
62 N. Talebloo, M. Gudi, N. Robertson and P. Wang, *Magn. Reson. Imaging*, 2020, **51**, 1659–1668.
63 P. Goodwill, E. Saritas, L. Croft, T. Kim, K. Krishnan, D. Schaffer and S. Conolly, *Adv. Mater.*, 2012, **24**, 3870–3877.
64 G. Song, M. Chen, Y. Zhang, L. Cui, H. Qu, X. Zheng, M. Wintermark, Z. Liu and J. Rao, *Nano Lett.*, 2018, **18**, 182–189.
65 B. R. Smith and S. S. Gambhir, *Chem. Rev.*, 2017, **117**, 901–986.
66 Z. Zhou and Z. Lu, *Adv. Drug Delivery Rev.*, 2017, **113**, 24–48.
67 J. Wolfram, M. Zhu, Y. Yang, J. Shen, E. Gentile, D. Paolino, M. Fresta, G. Nie, C. Chen, H. Shen, M. Ferrari and Y. Zhao, *Curr. Drug Targets*, 2015, **16**, 1671–1681.
68 V. Pansare, S. Hejazi, W. Faenza and R. Prud'homme, *Chem. Mater.*, 2012, **24**, 812–827.
69 G. Song, C. Liang, X. Yi, Q. Zhao, L. Cheng, K. Yang and Z. Liu, *Adv. Mater.*, 2016, **28**, 2716–2723.
70 Kenry, Y. Duan and B. Liu, *Adv. Mater.*, 2018, **30**, 1802394.
71 S. Zhu, R. Tian, A. Antaris, X. Chen and H. Dai, *Adv. Mater.*, 2019, **31**, e1900321.
72 H. Dai, X. Wang, J. Shao, W. Wang, X. Mou and X. Dong, *Small*, 2021, **17**, e2102646.
73 H. Dai, Z. Cheng, T. Zhang, W. Wang, J. Shao, W. Wang, Y. Zhao, X. Dong and L. Zhong, *Chin. Chem. Lett.*, 2021, DOI: 10.1016/j.cclet.2021.11.079.
74 D. Sheng, T. Liu, L. Deng, L. Zhang, X. Li, J. Xu, L. Hao, P. Li, H. Ran, H. Chen and Z. Wang, *Biomaterials*, 2018, **165**, 1–13.
75 C. Yue, P. Liu, M. Zheng, P. Zhao, Y. Wang, Y. Ma and L. Cai, *Biomaterials*, 2013, **34**, 6853–6861.
76 H. Han, H. Wang, Y. Chen, Z. Li, Y. Wang, Q. Jin and J. Ji, *Nanoscale*, 2016, **8**, 283–291.
77 N. Kosaka, M. Ogawa, P. L. Choyke, N. Karassina, C. Corona, M. McDougall, D. T. Lynch, C. C. Hoyt, R. M. Levenson, G. V. Los and H. Kobayashi, *Bioconjugate Chem.*, 2009, **20**, 1367–1374.
78 K. Choi, H. Chung, K. Min, H. Yoon, K. Kim, J. Park, I. Kwon and S. Jeong, *Biomaterials*, 2010, **31**, 106–114.
79 G. Abatangelo, V. Vindigni, G. Avruscio, L. Pandis and P. Brun, *Cells*, 2020, **9**, 1743.
80 M. Litwiniuk, A. Krejner, M. S. Speyrer, A. R. Gauto and T. Grzela, *Wounds*, 2016, **28**, 78–88.
81 J. M. Wickens, H. O. Alsaab, P. Kesharwani, K. Bhise, M. Amin, R. K. Tekade, U. Gupta and A. K. Iyer, *Drug Discovery Today*, 2017, **22**, 665–680.
82 S. Arpicco, P. Milla, B. Stella and F. Dosio, *Molecules*, 2014, **19**, 3193–3230.
83 B. Qi, A. Crawford, N. Wojtynek, M. Holmes, J. Souchek, G. Almeida-Porada, Q. Ly, S. Cohen, M. Hollingsworth and A. Mohs, *Nanomedicine*, 2018, **14**, 769–780.
84 D. M. Tacelosky, A. E. Creecy, S. S. Shanmugavelandy, J. P. Smith, D. F. Claxton, J. H. Adair, M. Kester and B. M. Barth, *Discovery Med.*, 2012, **13**, 275–285.
85 A. K. Burwell, L. J. Litkowski and D. C. Greenspan, *J. Dent. Res.*, 2009, **21**, 35–39.
86 G. Clawson, T. Abraham, W. Pan, X. Tang, S. Linton, C. McGovern, W. Loc, J. Smith, P. Butler, M. Kester, J. Adair and G. Matters, *Nucleic Acid Ther.*, 2017, **27**, 23–35.
87 G. Giordano, M. Pancione, N. Olivieri, P. Parcesepe, M. Velocci, T. Di Raimo, L. Coppola, G. Toffoli and M. R. D'Andrea, *World J. Gastroenterol.*, 2017, **23**, 5875–5886.
88 E. Kianfar, *J. Nanobiotechnol.*, 2021, **19**, 159.
89 Y. Ishima and T. Maruyama, *Yakugaku Zasshi*, 2016, **136**, 39–47.
90 H. Han, J. Wang, T. Chen, L. Yin, Q. Jin and J. Ji, *J. Colloid Interface Sci.*, 2017, **507**, 217–224.
91 M. Gisbert-Garzarán, D. Lozano and M. Vallet-Regí, *Int. J. Mol. Med.*, 2020, **21**, 9696.
92 S. Jafari, H. Derakhshankhah, L. Alaei, A. Fattahi, B. S. Varnamkhasti and A. A. Saboury, *Biomed. Pharmacother.*, 2019, **109**, 1100–1111.
93 M. Manzano and M. Vallet-Regí, *J. Mater. Sci. Mater. Med.*, 2018, **29**, 65.
94 A. Ravindran Girija and S. Balasubramanian, *Nanotheranostics*, 2019, **3**, 1–40.
95 H. Li, K. Li, Y. Dai, X. Xu, X. Cao, Q. Zeng, H. He, L. Pang, J. Liang, X. Chen and Y. Zhan, *Nanomedicine*, 2018, **14**, 1867–1877.
96 G. H. Glover, *Crit. Care Nurs. Clin. North Am.*, 2011, **22**, 133–139.
97 H. Yuan, Y. Zhao, C. Yang, C. Zhang and X. Zhang, *Sci. China: Chem.*, 2020, **63**, 924–935.
98 D. Zhu, F. Liu, L. Ma, D. Liu and Z. Wang, *Int. J. Mol. Sci.*, 2013, **14**, 10591–10607.
99 A. Heshmatzadeh Behzadi, Z. Farooq, J. H. Newhouse and M. R. Prince, *Medicine*, 2018, **97**, e0055.
100 J. Pellico, C. M. Ellis and J. J. Davis, *Contrast Media Mol. Imaging*, 2019, **2019**, 1845637.
101 S. M. Dadfar, K. Roemhild, N. I. Drude, S. von Stillfried, R. Knüchel, F. Kiessling and T. Lammers, *Adv. Drug Delivery Rev.*, 2019, **138**, 302–325.

102 S. Sammet, *Abdom. Radiol.*, 2016, **41**, 444–451.
103 H. Li and T. J. Meade, *J. Am. Chem. Soc.*, 2019, **141**, 17025–17041.
104 J. Lux and A. D. Sherry, *Curr. Opin. Chem. Biol.*, 2018, **45**, 121–130.
105 Q. Wang, J. Li, S. An, Y. Chen, C. Jiang and X. Wang, *Int. J. Nanomed.*, 2015, **10**, 4479–4490.
106 Y. He, W. Song, J. Lei, Z. Li, J. Cao, S. Huang, J. Meng, H. Xu, Z. Jin and H. Xue, *Acta Radiol.*, 2012, **53**, 1049–1058.
107 U. Mahajan, S. Teller, M. Sendler, R. Palankar, C. van den Brandt, T. Schwaiger, J. Kühn, S. Ribback, G. Glöckl, M. Evert, W. Weitschies, N. Hosten, F. Dombrowski, M. Delcea, F. Weiss, M. Lerch and J. Mayerle, *Gut*, 2016, **65**, 1838–1849.
108 L. Wang, H. Yin, R. Bi, G. Gao, K. Li and H. Liu, *J. Cell. Mol. Med.*, 2020, **24**, 5751–5757.
109 J. Zou, S. Chen, Y. Li, L. Zeng, G. Lian, J. Li, S. Chen, K. Huang and Y. Chen, *Nanoscale*, 2020, **12**, 4473–4490.
110 C. Cronin, P. Prakash and M. Blake, *Am. J. Roentgenol.*, 2010, **195**, W5–W13.
111 B. Yeh, P. FitzGerald, P. Edic, J. Lambert, R. Colborn, M. Marino, P. Evans, J. Roberts, Z. Wang, M. Wong and P. Bonitatibus, *Adv. Drug Delivery Rev.*, 2017, **113**, 201–222.
112 N. Lee, S. Choi and T. Hyeon, *Adv. Mater.*, 2013, **25**, 2641–2660.
113 J. Hsu, L. Nieves, O. Betzer, T. Sadan, P. Noël, R. Popovtzer and D. Cormode, *Wiley Interdiscip. Rev.: Nanomed. Nanobiotechnol.*, 2020, **12**, e1642.
114 A. L. Brown, P. C. Naha, V. Benavides-Montes, H. I. Litt, A. M. Goforth and D. P. Cormode, *Chem. Mater.*, 2014, **26**, 2266–2274.
115 Y. C. Dong, M. Hajfathalian, P. S. N. Maidment, J. C. Hsu, P. C. Naha, S. Si-Mohamed, M. Breuilly, J. Kim, P. Chhour, P. Douek, H. I. Litt and D. P. Cormode, *Sci. Rep.*, 2019, **9**, 14912.
116 R. D. Ross, L. E. Cole, J. M. Tilley and R. K. Roeder, *Chem. Mater.*, 2014, **26**, 1187–1194.
117 A. Sofuni, T. Tsuchiya and T. Itoi, *J. Med. Ultrason.*, 2020, **47**, 359–376.
118 D. Maresca, A. Lakshmanan, M. Abedi, A. Bar-Zion, A. Farhadi, G. J. Lu, J. O. Szablowski, D. Wu, S. Yoo and M. G. Shapiro, *Annu. Rev. Chem. Biomol. Eng.*, 2018, **9**, 229–252.
119 W. Chong, V. Papadopoulou and P. Dayton, *Abdom. Radiol.*, 2018, **43**, 762–772.
120 C. Dietrich and C. Jenssen, *Ultrasonography*, 2020, **39**, 105–113.
121 V. Paefgen, D. Doleschel and F. Kiessling, *Front. Pharmacol.*, 2015, **6**, 197.
122 G. Song, Y. Chao, Y. Chen, C. Liang, X. Yi, G. Yang, K. Yang, L. Cheng, Q. Zhang and Z. Liu, *Adv. Funct. Mater.*, 2016, **26**, 8243–8254.
123 P. Wang, F. Zhou, K. Guan, Y. Wang, X. Fu, Y. Yang, X. Yin, G. Song, X. Zhang and W. Tan, *Chem. Sci.*, 2019, **11**, 1299–1306.
124 G. Pirovano, S. Roberts, S. Kossatz and T. Reiner, *J. Nucl. Med.*, 2020, **61**, 1419–1427.
125 M. Wu and J. Shu, *Contrast Media Mol. Imaging*, 2018, **2018**, 1382183.
126 K. M. Bennett, J. Jo, H. Cabral, R. Bakalova and I. Aoki, *Adv. Drug Delivery Rev.*, 2014, **74**, 75–94.
127 X. Cai, Q. Zhu, Y. Zeng, Q. Zeng, X. Chen and Y. Zhan, *Int. J. Nanomed.*, 2019, **14**, 8321–8344.
128 J. R. Fink, M. Muzi, M. Peck and K. A. Krohn, *J. Nucl. Med.*, 2015, **56**, 1554–1561.
129 Q. Wang, H. Yan, Y. Jin, Z. Wang, W. Huang, J. Qiu, F. Kang, K. Wang, X. Zhao and J. Tian, *Biomaterials*, 2018, **183**, 173–184.
130 H. Li, P. Wang, W. Gong, Q. Wang, J. Zhou, W. Zhu and Y. Cheng, *Adv. Healthcare Mater.*, 2018, **7**, 1700912.
131 Y. Han, Y. An, G. Jia, X. Wang, C. He, Y. Ding and Q. Tang, *J. Nanobiotechnol.*, 2018, **16**, 7.
132 X. Huang, C. Fan, H. Zhu, W. Le, S. Cui, X. Chen, W. Li, F. Zhang, Y. Huang, D. Sh, Z. Cui, C. Shao and B. Chen, *Int. J. Nanomed.*, 2018, **13**, 2585–2599.
133 O. P. Medina, R. J. Tower, T. P. Medina, F. Ashkenani, L. Appold, M. Bötcher, L. Huber, O. Will, Q. Ling and C. Hauser, *Curr. Pharm. Des.*, 2022, **28**, 313–323.
134 P. Wang, B. Yoo, S. Sherman, P. Mukherjee, A. Ross, P. Pantazopoulos, V. Petkova, C. Farrar, Z. Medarova and A. Moore, *Int. J. Cancer*, 2016, **139**, 712–718.
135 Å. Barrefelt, Y. Zhao, M. K. Larsson, G. Egri, R. V. Kuiper, J. Hamm, M. Saghafian, K. Caidahl, T. B. Brismar, P. Aspelin, R. Heuchel, M. Muhammed, L. Dähne and M. Hassan, *Biochem. Biophys. Res. Commun.*, 2015, **464**, 737–742.
136 S. Tang, G. Huang, J. Liu, T. Liu, L. Treven, S. Song, C. Zhang, L. Pan and T. Zhang, *Eur. J. Radiol.*, 2011, **78**, 142–150.
137 Y. Zhao, F. Ye, T. Brismar, X. Li, R. He, R. Heuchel, R. El-Sayed, N. Feliu, W. Zheng, S. Oerther, J. Dutta, W. Parak, M. Muhammed and M. Hassan, *ACS Appl. Mater. Interfaces*, 2020, **12**, 53665–53681.
138 G. Song, M. Kenney, Y. S. Chen, X. Zheng, Y. Deng, Z. Chen, S. X. Wang, S. S. Gambhir, H. Dai and J. Rao, *Nat. Biomed. Eng.*, 2020, **4**, 325–334.
139 G. Song, X. Zheng, Y. Wang, X. Xia, S. Chu and J. Rao, *ACS Nano*, 2019, **13**, 7750–7758.
140 F. Chen, L. Teng, C. Lu, C. Zhang, Q. Rong, Y. Zhao, Y. Yang, Y. Wang, G. Song and X. Zhang, *Anal. Chem.*, 2020, **92**, 13452–13461.
141 P. Peddu, A. Quaglia, P. Kane and J. Karani, *Crit. Rev. Oncol. Hematol.*, 2009, **70**, 12–23.
142 C. J. Mclaren, D. Day, D. Croagh, A. Strickland and E. Segelov, in *Advances in Pancreatic Cancer*, ed. L. Rodrigo, 2019, ch. 4, pp. 73–94.
143 V. Blanco, T. Latif, Z. Chu and X. Qi, *Transl. Oncol.*, 2015, **8**, 196–203.
144 I. Steinberg, D. Huland, O. Vermesh, H. Frostig, W. Tummers and S. Gambhir, *Photoacoustics*, 2019, **14**, 77–98.